applied sciences

MDPI

Article

Salinity-Driven Modulation of Growth and FAME Composition in *Auxenochlorella protothecoides* for Industrial Applications

Thomas Morra [1], Samaneh Mohammadnejad [2], Veronica Lolli [3], Francesco Sansone [1,*], Ali Parsaeimehr [4], Giovanni Antonio Lutzu [2,*] and Alessandro Concas [5,6,*]

[1] Department of Chemistry, Life Sciences and Environmental Sustainability, University of Parma, Parco Area delle Scienze 11/A, 43124 Parma, Italy
[2] Teregroup Srl, Via David Livingstone 37, 41122 Modena, Italy
[3] Department of Food and Drug, University of Parma, Parco Area delle Scienze 27/A, 43124 Parma, Italy; veronica.lolli@unipr.it
[4] Department of Biology and Microbiology, South Dakota State University, Brookings, SD 57007, USA; ali.parsaeimehr@sdstate.edu
[5] Department of Mechanical, Chemical and Materials Engineering, University of Cagliari, Piazza d'Armi, 09123 Cagliari, Italy
[6] Interdepartmental Center of Environmental Science and Engineering (CINSA), University of Cagliari, Via San Giorgio 12, 09124 Cagliari, Italy
* Correspondence: francesco.sansone@unipr.it (F.S.); gianni.lutzu@teregroup.net (G.A.L.); alessandro.concas@unica.it (A.C.); Tel.: +39-0521-905458 (F.S.); +39-059-4823699 (G.A.L.); +39-070-6755078 (A.C.)

Abstract

Microalgal lipid production requires cultivation strategies that reduce freshwater demand while maintaining biomass productivity and improving the quality of fatty acid methyl ester (FAME) profiles for downstream applications. In this context, salinity is a relevant but still insufficiently characterized factor, particularly for *Auxenochlorella protothecoides*, whose response to salt stress in terms of growth dynamics, lipid productivity, and FAME composition remains poorly understood. This study investigated the effect of NaCl concentrations ranging from 0 to 50 g L^{-1} on the growth, lipid accumulation, FAME profile, and predicted biodiesel-related properties of *A. protothecoides*. Growth kinetics were described using logistic and Gaussian models. The highest carrying capacity was observed at 10 g L^{-1} NaCl, whereas the modeled optimum for specific growth rate occurred under moderate salinity, close to 20 g L^{-1} NaCl. Lipid analyses showed that C16–C18 fatty acids (FAs) dominated across treatments, accounting for more than 90% of total FAMEs, and that increasing salinity shifted the profile from a more saturated C16:0-rich composition toward higher proportions of unsaturated C18 FAs, particularly oleic and linoleic acids. Biodiesel property estimations indicated that mild salinity (5 g L^{-1}) improved some fuel-relevant parameters relative to the other salinity treatments, including cetane number, iodine value, cold-flow-related properties, and oxidative stability. Nevertheless, the predicted viscosity values were below the EN 14214 specification range for all treatments, and oxidative stability at 5 g L^{-1} only marginally met the European minimum requirement, indicating partial rather than full compliance with biodiesel standards. These findings indicate that salinity can be used as a practical tool to tune biomass production and lipid quality in *A. protothecoides*, supporting its potential use in microalgal biorefineries and oleochemical applications. Furthermore, the ability of the strain to tolerate saline conditions may support the future use of brackish water, seawater, or saline waste streams, potentially reducing freshwater demand; however, this environmental benefit was not quantified in the present study and should be validated through dedicated water-footprint or life-cycle assessment. Direct biodiesel application also remains limited by incomplete compliance with fuel standards, and further optimization

Check for updates

Academic Editor: George Aggelis

Received: 21 June 2026
Revised: 25 July 2026
Accepted: 3 August 2026
Published: 6 August 2026

Copyright: © 2026 by the authors. Licensee MDPI, Basel, Switzerland. This article is an open access article distributed under the terms and conditions of the Creative Commons Attribution (CC BY) license.

through cultivation in real saline or wastewater-based media, process scale-up, blending, or downstream upgrading will be required to improve industrial feasibility.

Keywords: *Auxenochlorella protothecoides*; salinity-driven lipid modulation; growth kinetics; fatty acid methyl esters; microalgal biorefinery; oleochemical applications; biodiesel properties; water-footprint reduction

1. Introduction

The transition toward renewable carbon sources has increased the interest in biodiesel and oleochemical feedstocks derived from biological lipids [1]. Among the available biomass resources, microalgae are particularly attractive because they can combine rapid growth, high lipid productivity, year-round cultivation, and reduced competition with arable land [2–4]. In addition, several microalgal species can be cultivated using low-quality waters or nutrient-rich waste streams, thereby improving the sustainability of lipid production systems [5–7].

Microalgal biodiesel consists mainly of fatty acid methyl esters (FAMEs), whose composition strongly determines fuel-relevant properties such as cetane number, viscosity, oxidative stability, iodine value, cold-flow behavior, and heating value [1,8,9]. Therefore, current research is not limited to maximizing lipid yield, but also aims to modulate the relative abundance of specific fatty acids (FAs) in order to improve the suitability of the resulting lipid fraction for biodiesel and other oleochemical applications [2,8–10].

On the other hand, beyond their use as biodiesel precursors, microalgal FAMEs are attracting increasing attention as renewable feedstocks for the oleochemical industry. Depending on chain length and degree of unsaturation, these compounds can be exploited for the synthesis of biodegradable lubricants, surfactants, plasticizers, coatings and bio-based polymer intermediates [11,12]. In particular, FAMEs' mixtures rich in C16–C18 mono- and polyunsaturated fatty acids (PUFA) are considered especially attractive for the production of epoxidized derivatives and specialty chemicals, thereby opening opportunities for the integration of biodiesel production within a broader microalgal biorefinery framework [11,12].

The goal of the current research is therefore twofold: to maximize overall lipid (and thus FAMEs) productivity while keeping cultivation costs low, and to tailor the FAME composition to meet the distinct requirements of different industrial applications. For instance, in biodiesel production, individual FAMEs directly influence critical fuel properties such as the cetane number, viscosity, oxidative stability, cold flow behavior, and heating value. Achieving a balanced FAME profile is essential to optimize both combustion performance and fuel stability [8,9]. A similar logic applies to other oleochemical industries, where FAME's relative content must be precisely adjusted depending on the final product's intended use.

Achieving these goals requires the careful selection of both an optimal microalgal strain and an efficient cultivation strategy. In this context, salinity represents a particularly relevant cultivation variable because it can influence both biomass accumulation and FA desaturation patterns, while also enabling the use of brackish or seawater-based media [13].

Salinity stress is particularly relevant because it acts simultaneously as an environmental constraint and as a metabolic regulator [14,15]. When exposed to increased external NaCl concentrations, microalgal cells must maintain osmotic balance, regulate intracellular ion concentrations, and prevent salt-induced oxidative damage [16]. These processes require energy and can reduce cell division under excessive stress [15]. However, mod-

erate salinity may also activate adaptive responses, including osmolyte accumulation, remodeling of membrane lipids, changes in FA desaturation, and redirection of carbon flux toward storage lipids such as triacylglycerols [15,16]. From a biotechnological perspective, this makes salinity a useful cultivation parameter because it can potentially tune both biomass productivity and lipid quality [14]. In addition, salinity-tolerant strains may be compatible with brackish water, seawater, or saline waste streams, although the practical environmental benefit of using such water sources requires dedicated water-footprint or life-cycle assessment [17].

Among oleaginous green microalgae, *Auxenochlorella protothecoides* has attracted considerable attention as a platform strain for lipid production because of its metabolic flexibility, high neutral lipid accumulation capacity, and suitability for different cultivation strategies [18]. Earlier studies, conducted when the species was still commonly referred to as *Chlorella protothecoides*, demonstrated its ability to accumulate high lipid fractions under heterotrophic conditions and to generate biodiesel-relevant FAME profiles dominated by medium- and long-chain fatty acids. Xu et al. reported crude lipid contents of about 55% in heterotrophically cultivated *C. protothecoides*, supporting its potential for biodiesel production. Pilot-scale work further confirmed the industrial relevance of this strain group, with heterotrophic cultivation of *A. protothecoides* in a 60 m^3 fermenter producing biomass at 3.81 g L^{-1} day^{-1} and reaching approximately 51% neutral lipid content [19]. In addition, *A. protothecoides* has been investigated for cultivation on alternative substrates and wastewater streams, indicating its possible integration into lower-cost and resource-efficient microalgal bioprocesses [20]. These features make the strain a suitable candidate for evaluating how environmental stressors can be used to modulate lipid yield and lipid quality. The selection of *A. protothecoides* in the present study was therefore based on three main criteria: its documented oleaginous character, its metabolic flexibility, and its potential compatibility with biorefinery-oriented cultivation strategies. Moreover, genomic and multi-omics studies have provided evidence for the metabolic basis of oil accumulation in this species, including regulation of carbon flux and FA biosynthesis pathways [21]. Despite this background, most available studies have focused on heterotrophic or mixotrophic lipid production, alternative carbon sources, wastewater cultivation, or biodiesel conversion. By contrast, the specific role of salinity as a controlled abiotic factor affecting both growth kinetics and FAME composition in *A. protothecoides* remains less clearly defined [22]. This represents an important knowledge gap because salinity may simultaneously influence biomass productivity, osmotic-stress responses, fatty-acid desaturation, and the suitability of the resulting lipid fraction for biodiesel or oleochemical applications. Accordingly, the 0–50 g L^{-1} NaCl gradient was selected to distinguish between freshwater control conditions, low-to-moderate brackish salinities, marine-like salinity, and hypersaline boundary conditions useful for defining the physiological tolerance and lipid-remodeling capacity of *A. protothecoides*.

Based on this knowledge gap, the present study was designed to test the hypothesis that salinity modulates both growth performance and lipid quality in *A. protothecoides* in a concentration-dependent manner. Specifically, we hypothesized that: (i) moderate salinity would enhance or maintain biomass accumulation and specific growth rate compared with freshwater and hypersaline conditions; (ii) salt stress would alter lipid accumulation and FAME productivity; and (iii) increasing salinity would remodel the FAME profile, particularly the balance between saturated and unsaturated C16–C18 FAs, thereby affecting the predicted suitability of the lipid fraction for biodiesel and oleochemical applications. To test these hypotheses, *A. protothecoides* was cultivated under a salinity gradient from 0 to 50 g L^{-1} NaCl, and biomass production, lipid content, FAME composition, and predicted biodiesel-related properties were evaluated. Accordingly, the 0–50 g L^{-1} NaCl gradient

was selected to distinguish between freshwater control conditions, practically relevant brackish/marine-like salinities, and hypersaline boundary conditions useful for defining the physiological tolerance and lipid-remodeling capacity of the strain.

Growth kinetics were further interpreted using logistic and Gaussian models to identify salinity-dependent changes in growth dynamics and to support future optimization of cultivation conditions.

2. Materials and Methods

2.1. Inocula and Culture Medium Preparation

The strain *A. protothecoides* 210-10a, used in this study, was obtained from the Culture Collection of Algae at the University of Göttingen, Göttingen, Germany (SAG). This strain was selected to ensure taxonomic traceability and reproducibility, since culture-collection strains provide a controlled biological starting point for evaluating salinity-dependent physiological and compositional responses. Cell maintenance and cultivation experiments were performed using Doucha Medium (DM), whose composition is provided in Table S1. DM was prepared by combining equal volumes of aqueous macronutrient stock solutions reported in Table S1 and subsequently diluting the mixture 100-fold with water to obtain DM 100X. The resulting macronutrient solution was sterilized by autoclaving using a Model 760 autoclave (ASAL, Cernusco s/N, Milan, MI, Italy). After sterilization and cooling, the micronutrient solutions were added aseptically under a laminar flow cabinet (ASAL AIR 700, Cernusco s/N, Milan, MI, Italy), reaching a final 1000-fold dilution.

The inoculum for the salinity experiments was obtained from a mother culture previously grown in a 1 L flask containing DM 100X. This culture was kept under controlled laboratory conditions at room temperature, illuminated with fluorescent lamps (Model T8 36 W IP20, CMI, Wipperfürth, Germany) providing 50 μmol m^{-2} s^{-1}, and continuously aerated to maintain suitable culture conditions and minimize contamination risk. Gas exchange was allowed while limiting external contamination by sealing the flask with a cotton cup. Culture development was followed spectrophotometrically by measuring OD750, and the inoculum was collected when the culture reached the late exponential phase for use in the subsequent experimental trials.

2.2. Cultivation Conditions and Experimental Setup

A. protothecoides was cultivated in 500 mL flasks, each containing 250 mL of DM 100X. The experiment included eight salinity conditions: 0, 5, 10, 20, 35, 40, 45, and 50 g L^{-1} NaCl. Each condition was performed in triplicate, resulting in a total of 24 independent experimental flasks. Continuous aeration was provided by sterile cannulas delivering atmospheric air (~0.03% v v^{-1} CO_2) through cotton plugs equipped with filters, as illustrated in Figure S1. Cultures were maintained at room temperature under white fluorescent illumination (50 μmol m^{-2} s^{-1}), with a 12:12 h light-dark photoperiod.

For the salinity-stress experiments, NaCl was added to DM 100X (post-autoclaving) to obtain final concentrations of 5, 10, 20, 35, 40, 45, and 50 g L^{-1}. The selected salinity range was designed as a broad screening gradient rather than as a set of exclusively industrial operating conditions. The control without NaCl represented freshwater cultivation, whereas 5–20 g L^{-1} NaCl covered low-to-moderate brackish conditions potentially relevant for reducing freshwater use. The 35 g L^{-1} NaCl treatment was included to approximate marine-like salinity, while 40–50 g L^{-1} NaCl were used as hypersaline stress conditions to define the upper tolerance limits of *A. protothecoides* and to assess whether strong osmotic stress could further modulate lipid and FAME composition. Therefore, the higher salinity treatments should be interpreted mainly as physiological boundary conditions, not as preferred industrial cultivation targets. Since NaCl supplementation does not fully

reproduce the complex ionic composition of seawater or saline wastewaters, future scale-up studies should validate these findings using real brackish, marine, or wastewater-based media. The treatment without NaCl supplementation, 0 g L^{-1} NaCl, was used as the freshwater control. Therefore, all salinity-dependent responses were evaluated relative to this control condition.

Control cultures were prepared without NaCl, and all treatments were performed in triplicate. Each experimental setup was inoculated at an initial biomass concentration of 0.1 g L^{-1}. Growth performance, biomass productivity, lipid accumulation, and fatty acid methyl esters (FAME) profiles were subsequently evaluated. Culture growth was monitored by measuring optical density (OD_{750}) and biomass concentration (g L^{-1}), while final dry weight, total lipid content, and FAME composition were determined at the end of the cultivation period.

2.3. Cell Growth and Dry Weight Determination

The growth of *A. protothecoides* was monitored daily for 27 consecutive days by measuring culture absorbance (ABS) at 750 nm using a spectrophotometer (ONDA V30 SCAN—UV VIS, ZetaLab, Padua, Italy), with distilled water serving as the blank. A calibration curve correlating dried biomass concentration with ABS values was established through regression analysis, enabling biomass estimation directly from ABS reading. The detailed gravimetric method for dry biomass determination has been described elsewhere [8]. Dry cell concentration (X_{dw} g L^{-1}) was calculated as

$$X_{dw} = \frac{W_2 - W_1}{V} \quad (1)$$

where $W_2 - W_1$ represents the net dry weight (g) of algal biomass, and V is the culture volume (L) used for the test.

2.4. Total Lipid Content Determination

Total lipid content, TLP_f (%wt), was determined gravimetrically using a chloroform/methanol extraction procedure derived from previous protocols [23,24] and specifically adapted for lyophilized algal biomass. At the end of the cultivation period, the algal suspension was centrifuged at 6500 g for 5 min using a Model 2560 Nakita centrifuge (Auxilab S.L., Berain, Spain) to separate the biomass pellet from the culture supernatant. The recovered pellet, without any additional washing step, was frozen at −80 °C for approximately 24 h and then lyophilized using a Lio1000P freeze-dryer (5 Pascal, Trezzano s/N, Milan, MI, Italy), following the procedure described in detail in [8]. All lipid extractions were carried out on freeze-dried biomass, with no use of wet material. Therefore, the procedure should be considered a modified chloroform/methanol gravimetric extraction for dry algal biomass rather than the classical Bligh–Dyer method developed for wet biological samples. Briefly, the lyophilized biomass was initially extracted with chloroform/methanol (1:2, *v*/*v*). Chloroform and an aqueous 1% NaCl solution were subsequently added to promote phase separation, resulting in a final chloroform/methanol/aqueous phase ratio of approximately 2:2:1.8 (*v*/*v*/*v*). Because the biomass contained no intrinsic water, the aqueous phase was entirely supplied by the added NaCl solution.

After thorough mixing, the samples were centrifuged at 6500 g for approximately 5 min. The lower chloroform phase containing the extracted lipids was carefully collected into a pre-weighed glass tube (m_0, mg), evaporated under nitrogen flow at 60 °C for 90 min using an HGC 244 HA evaporator (Hangzhou, China), and subsequently reweighed (m_1, mg). Total lipid content was finally calculated and expressed on a dry biomass basis.

No chloride or total chlorine analysis was performed on the harvested biomass, lipid extract, or FAME fraction. Therefore, the present analytical results describe lipid content and FAME composition under a standardized preparation procedure, but do not quantify possible inorganic chloride carryover from the saline culture medium.

2.5. FAMEs Determination

FAME analysis was carried out on lyophilized biomass using a modified procedure based on the method described by [25], with the full analytical protocol reported in [8]. In brief, the transesterification reaction was performed using toluene and 1% H_2SO_4 in anhydrous methanol. Toluene was used to improve the solubilization and methylation of non-polar lipid fractions, while the acidic methanolic solution promoted trans-methylation. Tricosanoic acid methyl ester ($CH_3(CH_2)_{21}COOCH_3$, ≥99.0%, GC; Sigma Aldrich, St. Louis, MO, USA), dissolved in hexane at a concentration of 1 mg mL^{-1}, was added as the internal standard. After derivatization, FAMEs were recovered by liquid–liquid extraction using hexane and a 5% NaCl aqueous solution. Following phase separation, the organic phase was collected and analyzed by gas chromatography–mass spectrometry using a 7820A Gas Chromatograph coupled to a 5977B Mass Spectrometer (Agilent Technologies, Palo Alto, CA, USA). The specific GC-MS configuration, including capillary column, carrier gas, injector mode, and detector parameters, is described in detail in [8]. Individual FAMEs were identified and quantified using a Supelco 37 Component FAME Mix® standard (Sigma Aldrich, Saint Louis, MO, USA), together with tricosanoic acid methyl ester (TAME) internal standard.

Quantification was performed by manual integration of chromatographic peak areas, using the TAME signal as reference after determining the response factor (RF) from the standard solution. Fatty acid (FA) abundance was expressed as mg per 100 mg of total FAMEs.

The percentage contribution of each FAME (% of total FAMEs) was calculated according to the following equation:

$$FAME_i(\%) = \frac{m_{FAME_i}}{\sum_{i=1}^{N} m_{FAME_i}} \quad (2)$$

where m FAMEi is the mass (mg) of the individual methyl ester FAMEi, and N is the total number of integrated methyl esters.

Each salinity condition was analyzed in triplicate for the sake of reproducibility, so three FA profiles were obtained for each salinity.

2.6. Data Analysis and Modeling

2.6.1. Statistical Analysis

All experiments were carried out in triplicate for each experimental set-up. Statistical analyses of biomass and lipid content, specific growth rate, lipid productivity, and FAME profile were performed using Excel 2607 or Python 3.14. In particular, mean values and standard deviations of the replicate experimental measurements were calculated using Microsoft Excel. All subsequent statistical analyses, including experimental data fitting, parameter optimization, and goodness-of-fit evaluation, were performed in Python using NumPy 1.18.0 and SciPy 1.16.0. Statistical differences between different salinity conditions were assessed by one-way analysis of variance (ANOVA) eventually followed by Tukey's honestly significant difference (HSD) test. Statistical significance was considered at the 95% confidence level ($p < 0.05$).

2.6.2. Growth Kinetics

To describe the experimental growth data, the logistic model was applied, as it provides a realistic representation of microalgal dynamics by incorporating both the exponential growth phase and the subsequent saturation associated with resource limitation. Unlike the simple exponential model, which fails to account for the deceleration in growth as cultures approach the carrying capacity, the logistic formulation captures the entire growth trajectory. Mathematically, the model is expressed as

$$X(t) = \frac{X_{\max}}{1 + \left(\frac{X_{\max} - X_0}{X_0}\right) e^{-\mu(t - t_0)}} \tag{3}$$

where $X\left(\mathrm{g\,L^{-1}}\right)$ is the biomass concentration at time t (days), $X_{max}\left(\mathrm{g\,L^{-1}}\right)$ is the carrying capacity (maximum biomass concentration), $\mu\left(\mathrm{day^{-1}}\right)$ the specific growth rate, $X_0\left(\mathrm{g\,L^{-1}}\right)$ is the initial biomass at the starting time t_0 (days).

The experimental data were fitted by adjusting only the parameters μ and X_{max}, while t_0 and X_0 were fixed at zero (0) and the measured initial biomass concentration, respectively. Consequently, the fitting procedure involved only two free parameters that were estimated by nonlinear least-squares regression using the Levenberg–Marquardt algorithm as implemented in the *curve_fit* routine of the SciPy library [26]. Parameter uncertainties were obtained from the covariance matrix of the fit, and model performance was assessed by the coefficient of determination (R^2).

2.6.3. Effect of Salinity

The effect of salinity on the specific growth rate μ is analyzed using a unimodal Gaussian model to fit the data of the obtained specific growth rates Vs the corresponding salinities.

$$\mu(S) = \mu_{\mathrm{opt}} \exp\left[-\frac{(S - S_{\mathrm{opt}})^2}{2\sigma^2}\right] \tag{4}$$

where $\mu\ (S)$ is the specific growth rate $\left(\mathrm{day^{-1}}\right)$ at salinity $S\left(\mathrm{g\,L^{-1}}\right)$, $\mu_{opt}\left(\mathrm{day^{-1}}\right)$ is the maximum specific growth rate at optimum salinity $S_{opt}\left(\mathrm{g\,L^{-1}}\right)$ while $\sigma\left(\mathrm{g\,L^{-1}}\right)$ is a tolerance parameter (spread of salinity response).

Also, in this case, model parameters were estimated by nonlinear least-squares regression using the Levenberg–Marquardt algorithm as implemented in the *curve_fit* routine of the SciPy library [26].

2.6.4. Analysis of *A. protothecoides* Biomass Productivity

The maximum biomass productivity was evaluated as the maximum slope of the growth curve:

$$P_{\max} = \max\left(\frac{\partial X}{\partial t}\right) \tag{5}$$

with P_{max} having units of $\mathrm{g\,L^{-1}day^{-1}}$. So to evaluate the maximum productivity, the second time derivative of X was first calculated as

$$\frac{\partial^2 X}{\partial t^2} = \mu^2 X\left(1 - \frac{X}{X_{\max}}\right)\left(1 - \frac{2X}{X_{\max}}\right) \tag{6}$$

and then set equal to zero to identify the value of X at which the slope of the growth curve is maximum, that is for $X = X_{max}/2$ where

$$P_{\max} = \frac{\mu X_{\max}}{4} \tag{7}$$

and the corresponding time is when the biomass crosses half of the carrying capacity (inflection point):

$$t_{\max} = t_0 + \frac{1}{\mu} \ln\left(\frac{X_{\max} - X_0}{X_0}\right) \tag{8}$$

It is important to note that the knowledge of the maximum productivity and the time at which it is reached provides useful insights into the optimal cultivation duration and the appropriate time for discharging the batch reactor.

2.6.5. Final Biomass and Lipid Productivity Calculations

Because lipid content was measured only at the harvest stage (27 days), lipid productivity could be assessed exclusively at the final time point. As a first step, biomass productivity at the end of the cultivation period, $P_f\left(\mathrm{g\,L^{-1}day^{-1}}\right)$, was extrapolated for each salinity condition using the logistic growth model previously described, according to the following equation:

$$P_f = \frac{X_f - X_0}{t_f - t_0} \tag{9}$$

where X_f and $X_0\left(\mathrm{g\,L^{-1}}\right)$ are final and initial biomass concentration, respectively, while t_f and $t_0(\mathrm{days})$ are the final and initial cultivation time, respectively. The value of P_f was then multiplied by the final lipid percentage TLP_f (%wt) to obtain the final lipid productivity LP_f $\left(\mathrm{g\,L^{-1}day^{-1}}\right)$; that is,

$$LP_f = P_f \cdot TLP_f \tag{10}$$

2.6.6. Principal Component Analysis (PCA) Based on FAMEs

To evaluate the effects of different salinity levels on the FAME profiles of the microalgae, a Principal Component Analysis (PCA) was performed. Prior to the multivariate analysis, data preprocessing was carried out to optimize dataset quality: FAMEs that were consistently below the detection limit or undetected across most of the experimental conditions were excluded from the dataset to avoid noise and artifacts in the statistical models.

The remaining data were normalized (mean-centered and scaled to unit variance) to account for differences in the magnitude of individual FA percentages. PCA was subsequently executed to reduce the dimensionality of the dataset and visualize sample clustering based on salinity levels. The optimal number of principal components (PCs) was determined based on eigenvalues and the cumulative percentage of explained variance (Scree plot). To identify the key FAs contributing significantly to the separation among groups, Variable Importance in Projection (VIP) scores were also evaluated, considering variables with a VIP score greater than 1.0 as significant contributors to the observed variance.

All multivariate statistical analyses, data filtering, and graphical representations were performed using OriginPro 2025 software (OriginLab Corporation, Northampton, MA, USA).

2.6.7. Estimation of FAME Mixture Properties

The potential biodiesel quality derived from the extracted lipids was evaluated based on the FAME composition. Key fuel properties, including density (ρ), kinematic viscosity (υ), saponification value (SV), high heating value (HHV), cetane number (CN), iodine value (IV), long-chain saturation factor (LCSF), degree of unsaturation (DU), cold filter plugging

point (CFPP), and oxidative stability (OS) were calculated using the equations reported elsewhere [27]. Additional parameters such as allylic position equivalent (APE), bis-allylic position equivalent (BAPE), cloud point (CP), and pour point (PP) were estimated using the Biodiesel Analyzer© software, version 2.2 [28].

3. Results and Discussion

3.1. Growth Performance Under Salinity Stress

3.1.1. Growth Dynamics

Figure 1 illustrates the time-dependent changes in *A. protothecoides* biomass concentration under varying salinity levels, clearly showing that growth performance was markedly affected by the salinity of the culture medium. Cultures exposed to moderate salinity conditions demonstrated the highest growth potential. At 10 and 20 g L^{-1} NaCl, biomass concentrations reached values of approximately 4.0–4.3 g L^{-1}, representing the optimal range for this strain. A concentration of 5 g L^{-1} NaCl also supported robust growth, with only a slight reduction in the final biomass yield compared to 10–20 g L^{-1} NaCl. Although cells grew efficiently in freshwater, the final biomass (~3.1 g L^{-1}) was markedly lower than in the moderate salinity treatments.

This suggests that *A. protothecoides* benefits from the presence of a certain ionic strength in the culture medium, which may stabilize osmotic balance and support ion transport mechanisms.

At 35 g L^{-1} NaCl, cultures still attained relatively high biomass (~3.4 g L^{-1}), although growth was reduced compared to the optimum salinity range. The tolerance to this salinity level underlines the halotolerant character of this species. Overall, *A. protothecoides* exhibited favorable growth under brackish to moderate salinity conditions, particularly between 10 and 20 g L^{-1} NaCl. This range is below typical seawater salinity, which is approximately 35 PSU, corresponding to about 35 g kg^{-1} total dissolved salts and often approximated as ~35 g L^{-1} in culture studies. In the present experiment, the 35 g L^{-1} NaCl treatment was therefore considered the marine-like salinity condition [29].

These findings are in agreement with previous observations, which showed that *A. protothecoides* remains metabolically active and responsive under moderate salinity levels (i.e., 10 g L^{-1}) [30]. Similar trends have also been reported for other species, such as *Chlorella zofingiensis*, where optimal biomass accumulation occurred at 15 g L^{-1} NaCl within a 15–60 g L^{-1} salinity range [8]. At higher salinities, growth performance was affected in a more complex way. At 40 and 45 g L^{-1} NaCl, final biomass accumulation was lower than under moderate salinity conditions, indicating a clear inhibitory effect of hypersaline stress. At 50 g L^{-1} NaCl, the fitted carrying capacity was close to that of the freshwater control; however, this apparent similarity in final biomass should not be interpreted as equivalent productivity, because the specific growth rate was lower and the maximum productivity was reached later. Thus, the 50 g L^{-1} treatment indicates that *A. protothecoides* can tolerate severe salinity stress, but with slower growth dynamics and reduced productivity compared with the most favorable salinity conditions.

Growth rates were lower, and the stationary phase was reached earlier than under less saline conditions, indicating that osmotic stress severely constrained cell metabolism. Both in the absence of NaCl and at very high salt concentration ($\geq$40 g L^{-1}), *A. protothecoides* growth performance declines substantially, likely due to energetic costs associated with osmoregulation, osmolyte accumulation, and ion toxicity, as previously suggested [30]. This response can be interpreted as the result of a balance between beneficial acclimation and stress-related metabolic cost. At low-to-moderate salinity, the presence of NaCl may improve ionic balance and stimulate adaptive metabolism without severely impairing cell division. Under these conditions, cells can maintain photosynthetic activity and

nutrient transport while activating protective mechanisms against osmotic imbalance [31]. Conversely, at hypersaline levels, a larger fraction of cellular energy is likely diverted toward ion homeostasis, compatible-solute synthesis, antioxidant defense, and repair of salt-induced damage. This diversion reduces the resources available for biomass formation, explaining why high salinity may still allow survival but does not necessarily support optimal productivity [16]. The experimental data so far discussed were fitted through the logistic model by suitably adjusting the values of only two parameters, i.e., X_{max} and μ, as described in Sections 2.6.2 and 2.6.3. The fitting results are presented in Figure 1, while Table 1 reports the corresponding optimal parameter values together with the coefficient of determination R^2.

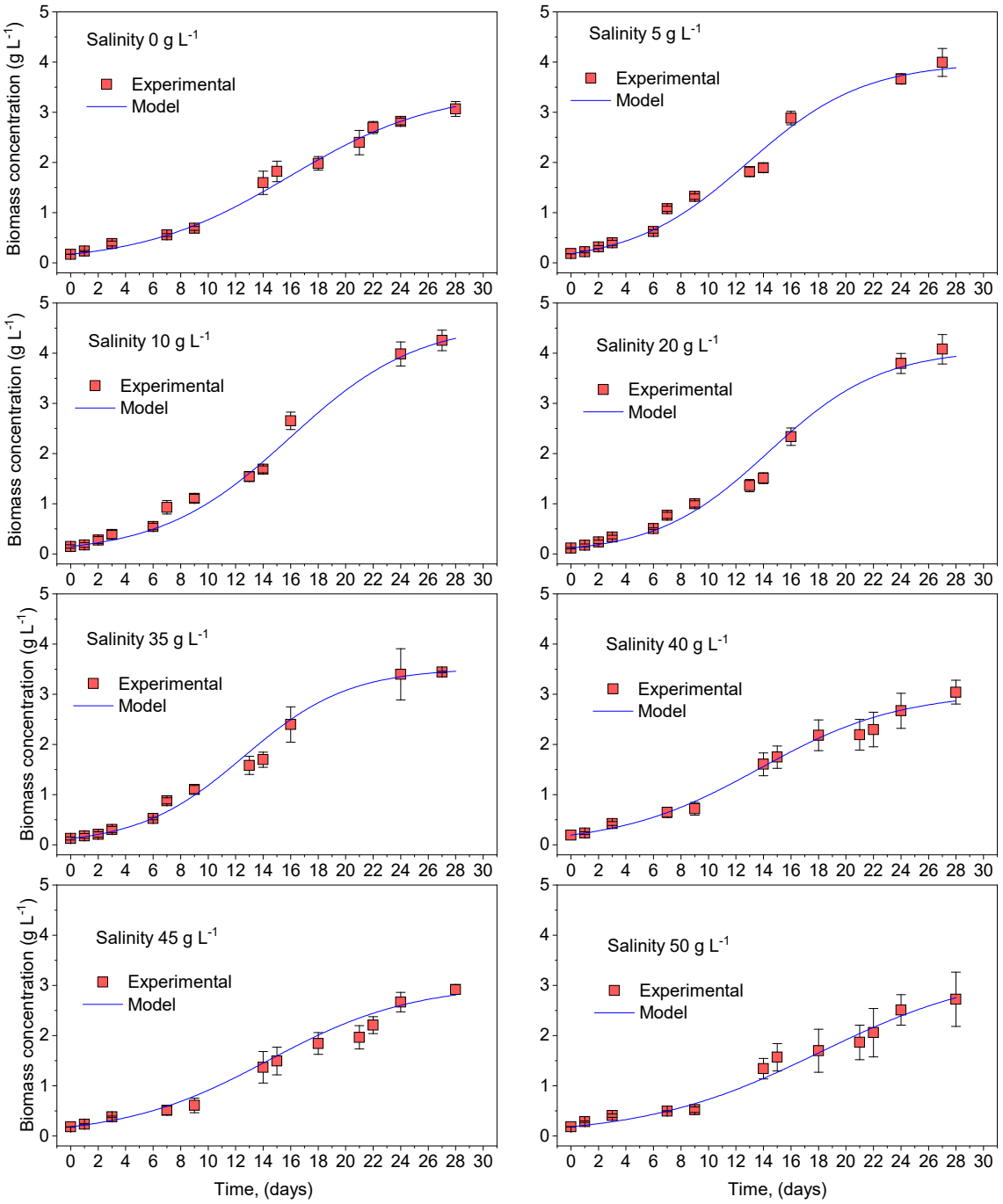

Figure 1. A. protothecoides growth dynamics at different salinities. Experimental results showing biomass concentration (g L−1) as a function of time (dots) and logistic model fittings (solid lines).

Table 1. Parameters of the logistic growth model under varying salinity conditions.

Salinity (g L^{-1})	t_0 (Days)	X_0 (g L^{-1})	μ (Day^{-1})	X_{max} (g L^{-1})	R^2 (/)
0	0	0.168 ± 0.002	0.18675 ± 0.00551	3.438 ± 0.136	0.993
5	0	0.181 ± 0.003	0.24184 ± 0.00444	3.804 ± 0.114	0.983
10	0	0.148 ± 0.033	0.21398 ± 0.00441	4.623 ± 0.231	0.987
20	0	0.117 ± 0.017	0.24896 ± 0.00465	3.806 ± 0.188	0.989
35	0	0.126 ± 0.032	0.26142 ± 0.00538	3.520 ± 0.021	0.989
40	0	0.194 ± 0.000	0.19578 ± 0.01269	3.042 ± 0.248	0.984
45	0	0.182 ± 0.003	0.19062 ± 0.01014	3.021 ± 0.138	0.988
50	0	0.183 ± 0.002	0.15723 ± 0.00456	3.338 ± 0.491	0.978

Note: Only X_{max} and μ were adjusted.

Compared with the freshwater control, salinity affected μ and X_{max} differently. The control showed μ = 0.187 day^{-1} and X_{max} = 3.438 g L^{-1}. At 5, 10, 20, and 35 g L^{-1} NaCl, μ increased relative to the control, with the strongest increase observed at 35 g L^{-1} NaCl. However, the highest X_{max} was obtained at 10 g L^{-1} NaCl, corresponding to an approximately 34.5% increase compared with the control. In contrast, hypersaline treatments at 40 and 45 g L^{-1} NaCl showed lower X_{max} values than the control, indicating reduced final biomass accumulation despite only moderate changes in μ.

The logistic model provided an excellent description of the experimental growth data, with coefficients of determination consistently above 0.97. However, salinity affected the specific growth rate, μ, and the carrying capacity, X_{max}, differently. The highest carrying capacity was obtained at 10 g L^{-1} NaCl, where X_{max} reached 4.623 ± 0.231 g L^{-1}, with a corresponding μ of 0.214 ± 0.004 day^{-1}. By contrast, at 20 g L^{-1} NaCl, μ was higher, reaching 0.249 ± 0.005 day^{-1}, whereas X_{max} was lower, at 3.806 ± 0.188 g L^{-1}. Therefore, 10 g L^{-1} NaCl was more favorable in terms of final biomass accumulation, while 20 g L^{-1} NaCl was closer to the salinity range associated with maximum growth-rate performance.

Interestingly, the highest observed μ value was recorded at 35 g L^{-1} NaCl, reaching 0.261 ± 0.005 day^{-1}; however, this was accompanied by a lower X_{max} of 3.520 ± 0.021 g L^{-1}. This indicates that higher salinity may accelerate the initial growth phase but also promote earlier saturation, likely due to increased metabolic costs associated with osmoregulation. Accordingly, the term "optimum salinity" should be interpreted as criterion-dependent: 10 g L^{-1} NaCl maximized carrying capacity, whereas the Gaussian model identified an optimum of 20.9 ± 0.7 g L^{-1} specifically for the smoothed μ response.

3.1.2. Effect of Salinity on the Growth Rate

The growth rate values obtained by fitting the experimental data with the logistic model were plotted against the corresponding salinity levels, as shown in Figure 2.

The data indicate an optimal salinity, generally between 5 and 35 g L^{-1}, with growth rates decreasing at salinities below or above this range. To better characterize the effect of salinity on the specific growth rate (μ), a unimodal Gaussian model was subsequently used to fit the data, as previously described (2.7). It can also be observed from Figure 2 that the fitted Gaussian model provides an excellent description of the experimental data, yielding an optimal salinity of 20.9 ± 0.7 g L^{-1}, an optimal μ of 0.245 ± 0.005 day^{-1}, and a tolerance parameter of 30 ± 2 g L^{-1} (Table S2). However, this salinity optimum of 20.9 ± 0.7 g L^{-1} refers specifically to the modeled specific growth-rate response and should not be interpreted as the salinity maximizing final biomass accumulation.

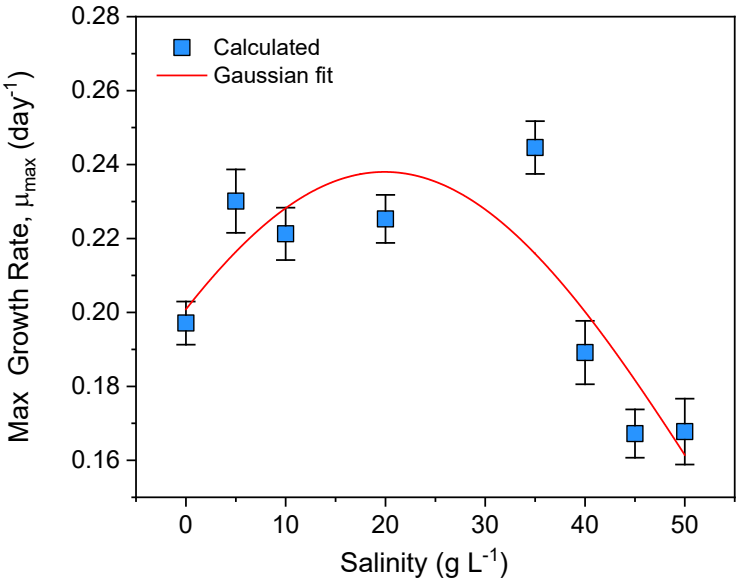

Figure 2. Effect of salinity on the specific growth rate (μ) and fitting through a Gaussian model.

In addition, the coefficient of determination (R^2) demonstrates excellent agreement between the experimental data and the fitted curve, confirming the suitability of the Gaussian model for describing the system. Such a unimodal response is typical of halotolerant or euryhaline species that maintain growth across wide salinity ranges [32]. The extrapolated maximum specific growth rate (0.245 day^{-1}) was within the range reported for other lipid-producing microalgae grown under controlled batch culture conditions [32,33].

The optimum salinity estimated here (about 21 g L^{-1}) is comparable to that of moderately halotolerant strains. For instance, *Nannochloropsis oculata* grows better at about 25 g L^{-1} [34], while *Dunaliella salina* tolerates 10–300 g L^{-1} but performs maximally at 30–40 g L^{-1} [35].

By contrast, the slightly lower optimum found in this work suggests adaptation to brackish conditions, while the persistence of growth up to 45–50 g L^{-1} indicates efficient osmotic regulation, likely through compatible solutes such as glycerol, a mechanism well-documented in extremotolerant taxa [32,35]. The observed salinity response of *A. protothecoides* represents a potential advantage for large-scale cultivation, as it reduces dependence on freshwater resources while also enabling enhanced lipid production, as further discussed in the following sections of this work.

3.1.3. Biomass Productivity

The effect of salinity on maximum biomass productivity is shown in Figure 3, while Table 2 indicates the time at which these maxima were reached.

Among the tested conditions, 35 g L^{-1} NaCl showed higher maximum biomass productivity than the control; however, because post hoc statistical groupings are not reported in Figure 3 or Table 2, this difference is described here as a trend rather than as a statistically confirmed effect. Apart from this apparent increase, salinity did not markedly alter maximum biomass productivity at the inflection point of the growth curve. These results suggest that moderate-to-marine salinity may support biomass productivity in *A. protothecoides*, but the strength of this effect requires explicit statistical support.

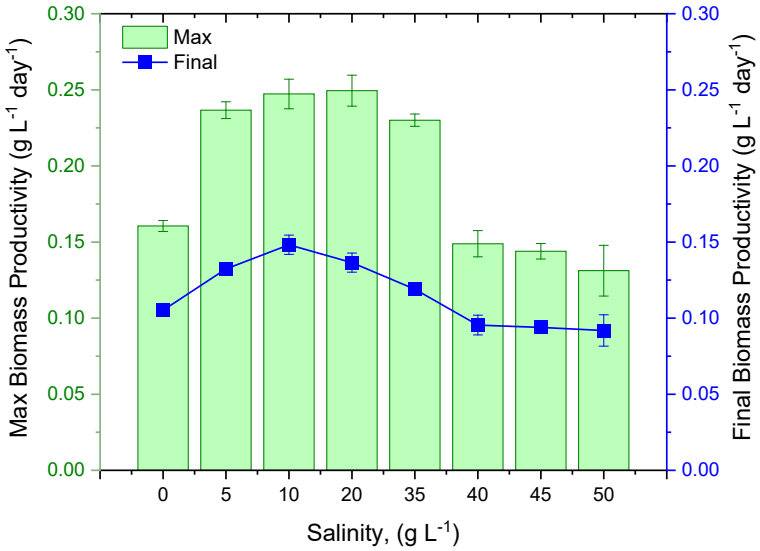

Figure 3. Effect of salinity on maximum instantaneous and final (after 27 days) biomass productivity of *A. protothecoides* cultures.

Table 2. Analysis of maximum biomass productivity and the time when they are achieved.

$Salinity\,(\mathbf{g\ L^{-1}})$	$P_{max}\left(\mathbf{g\ L^{-1}day^{-1}}\right)$	$t_{max}\,(\mathbf{day})$
0	0.160 ± 0.004	15.92 ± 0.67
5	0.230 ± 0.005	12.39 ± 0.33
10	0.247 ± 0.010	15.93 ± 0.53
20	0.237 ± 0.010	13.86 ± 0.42
35	0.230 ± 0.004	12.61 ± 0.28
40	0.149 ± 0.009	13.77 ± 1.26
45	0.144 ± 0.005	14.44 ± 0.98
50	0.131 ± 0.017	18.07 ± 1.45

At intermediate salinity values (5–20 g L^{-1}), productivity remained slightly above the control but without significant differences, whereas hypersaline conditions (>40 g L^{-1}) resulted in reduced productivity, even though measurable growth was still observed. Similarity in final biomass between 0 and 50 g L^{-1} NaCl does not imply similar process performance, since industrial productivity depends on both biomass concentration and the time required to reach it. A similar trend to that of the maximum instantaneous productivity was observed for the final productivity. However, lower overall values were achieved, indeed at the optimal salinity level, i.e., 10 g L^{-1}, the final productivity was approximately 0.15 g L^{-1} day^{-1}.

These results are consistent with the behavior of halotolerant strains such as *N. oculata*, which have been reported to achieve peak productivity at around 30 g L^{-1} salinity before declining at higher concentrations [34]. The decline observed under hypersaline conditions is in line with the well-established physiological responses of microalgae to osmotic stress, where excessive ion concentrations compromise photosynthetic efficiency and cellular metabolism [35]. Overall, the results confirm the euryhaline nature of *A. prototechoides* and highlight the potential of moderate salinity as an operational lever to optimize biomass production.

3.2. Lipid Production and FAME Composition

3.2.1. Lipid Content and Productivity

The total lipid content TLP_f (%wt) of *A. protothecoides* was quantified at the end of the cultivation period. The results reported in Figure 4 suggest that salinity exerted a clear influence on lipid accumulation.

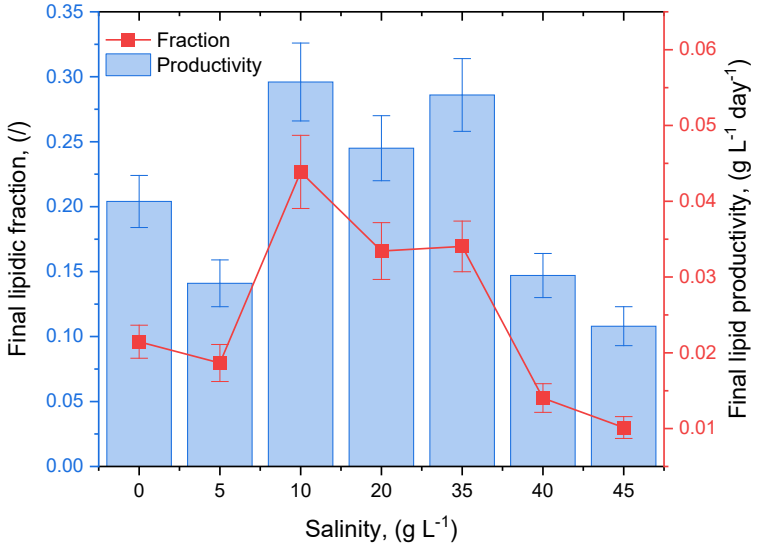

Figure 4. Effect of salinity on lipid content and total final (after 27 days) lipid productivity of *A. protothecoides* cultures.

However, statistical comparisons revealed that a significant difference from the control (0 g L^{-1}) was observed only at the highest salinity tested (50 g L^{-1}). Intermediate salinities (5–35 g L^{-1}) did not lead to statistically meaningful deviations from the freshwater control. From a biological perspective, these results suggest that lipid accumulation is primarily triggered by extreme osmotic stress, while moderate salinity changes have little effect on the lipid profile. This pattern partially aligns with the well-documented phenomenon of stress-induced lipid accumulation in microalgae: under unfavorable conditions, cells redirect carbon flux away from growth and toward neutral lipid storage as an adaptive mechanism, especially in the form of triacylglycerol (TAG) [36].

On the other hand, our results indicate that this effect occurs only at extremely high salinity levels (50 g L^{-1}). Salinity stress is known to cause oxidative imbalance and metabolic shift, ultimately enhancing TAG accumulation despite reduced cellular proliferation [37]. These findings confirm that while hypersaline conditions can boost lipid fraction, they typically come with a trade-off in biomass yield, highlighting the importance of balancing stress induction and productivity for biotechnological applications.

When calculating final biomass (P_f) and lipid productivities (LP_f) as earlier reported, the results shown in Figure 4 were obtained. Consistent with the growth behavior previously described, these results further indicate that *A. protothecoides* modulates its metabolism in response to salinity, with osmotic stress influencing both biomass formation and lipid accumulation.

Figure 4 reveals that Pf increases with milder salinity, peaking at 10 g L^{-1}, with only minor differences at other intermediate concentrations. This is also followed by a notable drop at 50 g L^{-1}, suggesting that excessive salinity significantly suppresses growth [30]. In contrast, LP_f (Figure 4) exhibited a different pattern, generally increasing with salinity, reaching its maximum at 50 g L^{-1}, despite slight decreases at 40–45 g L^{-1}. These findings suggest that higher salinity shifts metabolism towards lipid accumulation, but at the expense of reduced growth, indicating a salinity-dependent reallocation of resources. This

metabolic shift under hypersaline stress has been described in *Dunaliella* and *Monoraphidium* strains, where salinity-induced oxidative stress promotes TAG accumulation at the expense of cell division [38,39]. Overall, the results in Figure 4 emphasize that the optimal conditions for maximizing LP_f differ from those favoring biomass accumulation, underlining the importance of fine-tuning stress intensity in biofuel-oriented cultivation strategies.

3.2.2. Salinity-Induced Changes in the FAME Profile

It is well-documented that the suitability of microalgal biomass for biodiesel production is strongly influenced by the chain length and degree of unsaturation of its FAs, which determine compliance with international fuel standards [40,41]. The effect of salinity on FAME composition is mechanistically relevant because membrane lipids are among the first cellular targets of osmotic stress. Increased external salinity can reduce water availability, disturb ion gradients, and promote oxidative stress [31]. To counteract these effects, microalgae may adjust membrane fluidity by modifying the ratio between SFAs and UFAs. An increase in UFAs, especially C18:1 and C18:2, can improve membrane flexibility and help preserve the function of photosynthetic membranes, transport proteins, and other membrane-associated processes under osmotic stress [42]. At the same time, severe salinity can promote the accumulation of neutral lipids, mainly triacylglycerols, as a way to store excess carbon and reduce oxidative pressure. Therefore, salinity stress can be advantageous when it induces lipid remodeling without strongly suppressing growth, but it becomes detrimental when the energetic cost of stress tolerance exceeds the metabolic benefit.

To assess this, the FAs of *A. protothecoides* were transesterified and analyzed after 27 days of cultivation. The full results of these analyses are provided in the Supplementary Information (Table S3). The FAMEs profile of *A. protothecoides* was consistently characterized by higher concentrations of C16–C18 FA species across all salinity conditions (0–50 g L^{-1} NaCl). The major FAs were palmitic (C16:0), stearic (C18:0), oleic (OA, C18:1, cis-9), elaidic (C18:1, trans-9), and linoleic acid (LA, C18:2, n-6), which together accounted for the majority of the lipid fraction. In contrast, long-chain FAs, such as C20:0 and C24:0 or minor FA species, were present at low concentrations and remained largely unaffected by salt stress. Figure 5 illustrates the changes in the FAME profile of the FAs most affected by the tested conditions. Salinity induced significant and distinct shifts within the dominant C16–C18 FA pool. Palmitic acid (C16:0), the most concentrated FA in the control (36 ± 8% at 0 g L^{-1}), decreased considerably under salt stress, dropping to 25 ± 2% at 5 g L^{-1} and stabilizing around 20–22% at higher salinities (e.g., 21 ± 2% at 35 g L^{-1}).

LA exhibited the most pronounced increase, rising from 13± 2% at 0 g L^{-1} to 21± 3% at 5 g L^{-1}, peaking at 28.8 ± 0.6% at 20 g L^{-1}, and remaining elevated at 50 g L^{-1} (24.75 ± 0.70%). Elaidic acid (C18:1, trans-9), starting from 8 ± 3% in the control, decreased sharply to 3.7 ± 1.5% when salinity was augmented to 5 g L^{-1}, then re-increased moderately at intermediate salinities, before achieving a value of 6.52 ± 0.05% at 50 g L^{-1} of salinity.

Similarly, OA first increased sharply (from 13 ± 3% to 24 ± 3%) when salinity passed from 0 to 5 g L^{-1}, then slightly decreased when it was further increased up to 45 g L^{-1}. Then, the final increase from 45 to 50 g L^{-1} determined a re-increase in OA to 23.9 ± 0.8%. Stearic acid (C18:0) displayed variable responses: it decreased slightly at 5 g L^{-1} (13 ± 4%), remained relatively stable (~12–13%) across most salinity treatments, and peaked at 17 ± 2% at 45 g L^{-1} before returning to 12.55 ± 0.75% at 50 g L^{-1}. In Table 3, FAs were grouped into broader categories.

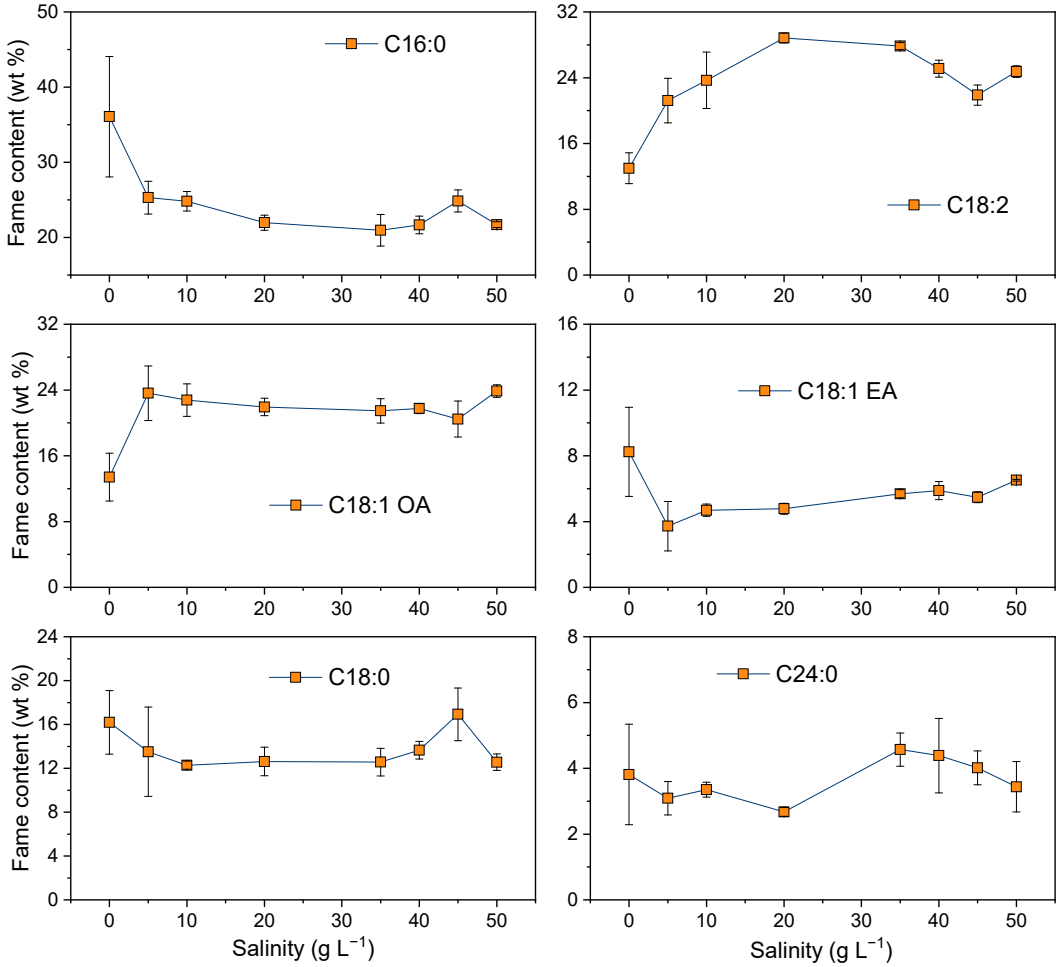

Figure 5. Effect of salinity on FAMEs of *A. prototechoides* mostly affected by osmotic stress.

Table 3. Impact of salinity (g L^{-1}) on FAME categories: saturated fatty acids (SFA), monounsaturated fatty acids (MUFA), polyunsaturated fatty acids (PUFA), C16–C18 FAs, and the UFA/SFA ratio.

Salinity (g L^{-1})	SFA (%wt)	MUFA (%wt)	PUFA (%wt)	C16–C18 (%wt)	UFA/SFA (/)
0	60.00 ± 9.00	25.00 ± 4.00	15.00± 6.00	90.00 ± 5.00	0.70 ± 0.30
5	44.99 ± 5.21	30.77 ± 2.92	24.25 ± 3.51	89.06 ± 0.89	1.24 ± 0.28
10	43.29 ± 1.36	30.15 ± 1.41	26.57 ± 2.75	89.24 ± 4.39	1.31 ± 0.07
20	39.88 ± 1.51	30.54 ± 1.97	29.58 ± 0.50	92.43 ± 0.66	1.51 ± 0.09
35	40.36 ± 2.15	31.40 ± 1.48	28.25 ± 0.67	91.26 ± 2.37	1.48 ± 0.13
40	42.75 ± 1.25	31.92 ± 1.2	25.33 ± 0.67	91.03 ± 1.33	1.34 ± 0.07
45	48.39 ± 3.55	29.71 ± 2.5	21.89 ± 1.23	92.36 ± 0.24	1.07 ± 0.15
50	40.07 ± 1.38	35.03 ± 0.92	24.89 ± 0.81	92.79 ± 0.58	1.50 ± 0.09

Saturated fatty acids (SFAs) decreased from 60 ± 9% at 0 g L^{-1} to 39.9 ± 1.5% at 20 g L^{-1}, while both monounsaturated (MUFAs) and polyunsaturated fatty acids (PUFAs) increased significantly. MUFA rose from 25 ± 4% at 0 g L^{-1} to approximately 30% under saline conditions, whereas PUFA nearly doubled, rising from 15 ± 6% in the control to 29.6 ± 0.5% at 20 g L^{-1}. Notably, the overall proportion of C16–C18 FAs remained largely stable (≈89–90% of the total), indicating that salinity altered the degree of unsaturation without affecting the chain-length distribution. The UFA/SFA ratio increased from 0.7 ± 0.3 at 0 g L^{-1} to 1.51 ± 0.09 at 20 g L^{-1}, clearly reflecting a metabolic shift from saturated to unsaturated lipids.

These results indicate that salinity induced a marked remodeling of the FA profile, shifting lipid composition from saturated species, particularly C16:0, toward more unsaturated C18 FAs such as C18:1 and C18:2 LA. Interestingly, although the degree of unsaturation changed substantially, the overall proportion of C16–C18 FAs remained relatively constant across the investigated salinity range.

This suggests that salinity mainly affected desaturation pathways rather than the chain-length distribution of FA biosynthesis. In particular, the strong increase in C18:2 LA and the moderate enrichment in C18:1 may reflect enhanced activity of Δ12- and Δ9-desaturases under osmotic stress conditions. The occurrence of elaidic acid (C18:1, trans-9) may additionally indicate stress-induced isomerization phenomena or selective incorporation of trans isomers into storage lipids. From a physiological perspective, the accumulation of unsaturated C18 species is consistent with the need to preserve membrane fluidity and maintain photosynthetic and transport functions under hyperosmotic environments, since MUFA and PUFA generally enhance membrane flexibility compared with saturated C16:0 species [43]. A scheme of the main possible effects of salinity on *A. protothecoides* FAMEs is shown in Figure 6.

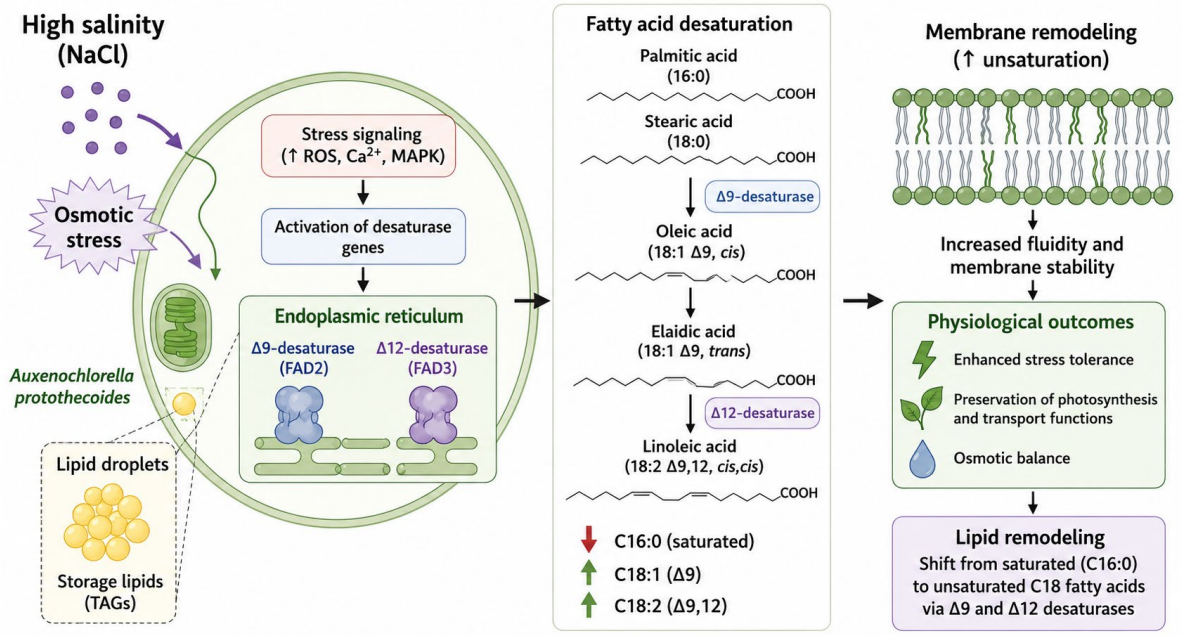

Figure 6. Scheme of the main effects of osmotic stress on the FAs of A. protothecoides. Symbol ↓ represents underexpression and ↑ overexpression.

Our findings are consistent with previous reports for other green microalgae. In *Scenedesmus* sp., salt stress similarly reduced C16:0 levels while increasing unsaturated C18 fractions, particularly C18:1 and C18:2, through desaturation-mediated lipid remodeling [44]. Similar salinity-induced lipid remodeling has been reported in other green microalgae. For example, Salama et al. observed changes in biomass, lipid content, and FA composition in *Chlamydomonas mexicana* and *Scenedesmus obliquus* grown under salt stress, while comparable increases in UFA fractions have also been reported in *Tetraselmis subcordiformis* under abiotic stress conditions [45,46]. In *Chromochloris zofingiensis*, transcriptomic analyses revealed salt-induced upregulation of Δ9- and Δ12-desaturases, consistent with the accumulation of C18:1 and C18:2 in both structural and storage lipids [47]. Likewise, in the halotolerant model organism *Dunaliella salina*, lipid remodeling under salt stress is well-documented, with increased unsaturation complementing its glycerol-based osmoregulatory strategy [48].

In addition, species-specific variability should also be considered. For instance, in *Nannochloropsis*, long-chain PUFAs such as EPA (C20:5, n-3) are often more strongly influenced by temperature and nutrient availability than by salinity [49,50].

In *Chlorella* species, responses can be more complex, with some strains exhibiting less pronounced enrichment of C18:2 under salt stress. Nevertheless, the consistent increase in C18:2 LA, along with the observed rise in the UFA/SFA ratio (Table 3), highlights the central role of desaturation-driven alteration of C18 FAs as a conserved adaptive response to salinity.

Overall, the data indicate that although the FAME profile remains primarily composed of C16–C18 species, salinity stress induces a pronounced alteration within this group, shifting the balance from saturated to unsaturated FAs. This lipid remodeling likely contributes to acclimation by maintaining membrane fluidity, while also carrying biotechnological implications. Increased unsaturation may improve the cold-flow properties of biodiesel derived from biomass, but could concurrently reduce its oxidative stability.

3.2.3. Multivariate Analysis of FAME Composition

Figure 7 shows the results of PCA providing a multivariate description of how FAME profiles respond to increasing salinity levels. The first two principal components explained 48.7% of the total variance, with PC1 and PC2 accounting for 26.8% and 21.9%, respectively. Therefore, although the PC1–PC2 projection is useful for visualizing the main compositional trends, it represents less than half of the total dataset variance and should be interpreted with caution. Within this two-dimensional projection, samples tended to distribute according to salinity level, with the 0 g L^{-1} group positioned separately from most salt-treated samples and the 5 g L^{-1} treatment showing an intermediate shift. Samples exposed to intermediate and high salinity generally moved toward the opposite side of PC1, suggesting that salinity contributed to a progressive remodeling of the FAME profile. However, because 51.3% of the variance was retained in higher-order components, this apparent separation should be considered a partial trend rather than definitive evidence of complete group discrimination.

The loading plot (Figure 7C) indicates that the separation along PC1 was mainly associated with variations in the dominant C16–C18 FAs, particularly C16:0, C18:1, and C18:2. However, the sign of the loading should not be interpreted directly as an increase or decrease with salinity, because PCA axes are sign-arbitrary and must be interpreted together with the score distribution. In agreement with the univariate FAME data, C16:0 contributed to the separation mainly because it was more abundant in the control and low-salinity samples and decreased under salt stress. Conversely, C18:2 LA, and to a lesser extent C18:1, were associated with the salinity-induced shift in FAME composition, reflecting the enrichment of unsaturated C18 species under osmotic stress. Therefore, PC1 should be interpreted as capturing a compositional transition from a more saturated C16:0-rich profile toward a more unsaturated C18-enriched profile, rather than as indicating that all positively loaded FAs increased with salinity. PC2 contributed to additional separation among treatments, although its interpretation should be considered secondary and exploratory.

The VIP (Variable Importance in Projection) analysis in Figure 7D indicates that most FAs exhibited VIP values close to or above 1, suggesting that they all contributed substantially to the discrimination among salinity treatments. In particular, the dominant C16–C18 FAs (e.g., C16:0, C18:1, and C18:2) showed high importance, confirming that salinity-induced remodeling of the major FA pool was the primary factor driving the observed differences in the FAME profile of *A. protothecoides*.

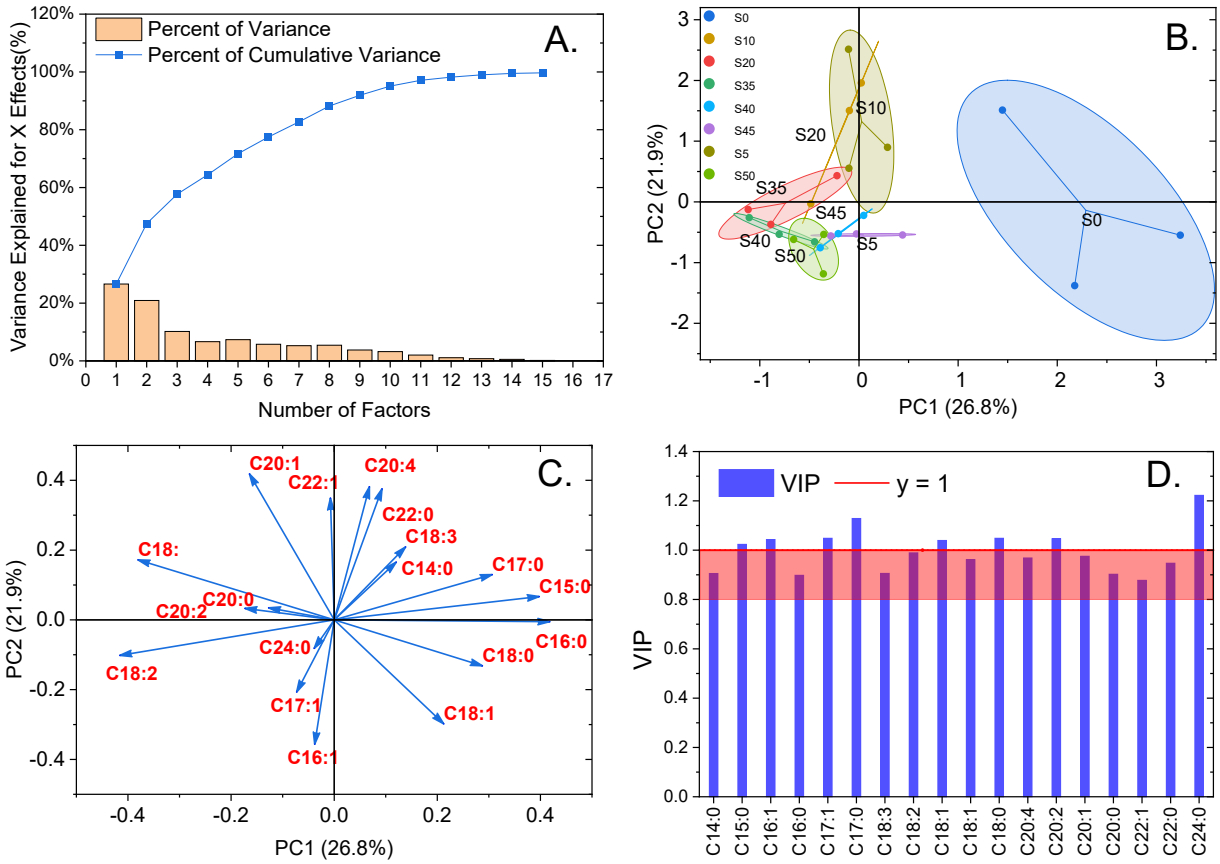

Figure 7. Principal component analysis (PCA) of FA composition under different salinity levels. (**A**) Scree plot; (**B**) score plot; (**C**) loading plot; (**D**) VIP plot.

It is important to note that the loading plot and VIP analysis were used only to identify the variables contributing most strongly to the variance captured in the PC1–PC2 space. In this projection, major C16–C18 FAs, including C16:0, C18:1, and C18:2, contributed substantially to the observed salinity-related trend. This is consistent with the univariate FAME data, which showed salinity-dependent changes mainly within the dominant C16–C18 fraction. Nevertheless, because the first two principal components accounted for only 48.7% of the total variance, these FAMEs should be interpreted as the main contributors to the projected PCA pattern, rather than as exhaustive drivers of the full multivariate variability.

The observed shift in FA composition with increasing salinity is consistent with well-documented osmoadaptive responses in microalgae and other photosynthetic microorganisms. Increased proportions of UFAs, particularly C18:2 LA and C18:1 species, have been reported as a mechanism to maintain membrane fluidity under hyperosmotic stress, thereby preserving photosynthetic efficiency and nutrient transport [50,51]. The strong contribution of C16:0 to PC1 suggests that saturated FA synthesis also plays a role, potentially reflecting adjustments in storage lipid pools or de novo FA biosynthesis under salinity stress. Interestingly, the discrimination along PC2 at 20 g L^{-1} suggests a non-linear response, possibly indicating a threshold at which stress signaling pathways are activated before full acclimation occurs. Together, these findings support the view that FA remodeling is a central component of the adaptive strategy to salinity and highlight the utility of PCA combined with supervised feature selection for uncovering dose-dependent metabolic responses in complex lipidomic datasets.

3.3. Predicted Properties and Potential Applications of the FAME Profile

3.3.1. Predicted Biodiesel Properties

Biodiesel quality is strongly influenced by the FAs composition of the feedstock, as chain length, degree of unsaturation, and branching determine key fuel properties [52]. In this context, C16:0 is particularly favorable for biodiesel synthesis, and the oil of *A. protothecoides*, with its high C16:0 content, represents a promising feedstock. Under low salinity conditions, C16:0 levels were elevated (25.30% at 5 g L^{-1} NaCl and 24.82% at 10 g L^{-1} NaCl), indicating that moderate salt concentrations can effectively enhance the accumulation of FAs relevant for biodiesel production. Overall, the FAME profile of *A. protothecoides* was composed mainly of C16–C18 FAs (>90%), with oleic (C18:1 ω-9) and linoleic acid (C18:2 ω-6) exhibiting substantial representation across treatments (20.46–23.87% and 21.23–28.84%, respectively). The degree of unsaturation ranged from 51.79% at 45 g L^{-1} NaCl to 60.45% at 35 g L^{-1} NaCl, confirming that UFAs constitute the major fraction of the lipid pool (Table 4). Given the close relationship between biodiesel properties and FAME composition, this lipid profile was further evaluated using Biodiesel Analyzer© Ver. 2.2 [28].

Table 4. Evaluation of the composition of the biodiesel obtainable using FAMEs from *A. prototechoides* cultivated under different salt stress conditions.

	Salinity Level							
Parameter	**0 g L^{-1} (CTRL)**	**5 g L^{-1}**	**10 g L^{-1}**	**20 g L^{-1}**	**35 g L^{-1}**	**40 g L^{-1}**	**45 g L^{-1}**	**50 g L^{-1}**
DU	57.35	76.19	81.00	82.9	80.80	75.61	67.64	77.18
SV	200.16	197.27	197.84	192.75	188.84	188.65	190.85	188
IV	60.96	73.56	79.17	75.07	73.21	68.56	61.32	70.02
CN	59.85	57.42	56.07	57.73	58.73	59.81	61.1	59.58
LCSF	21.52	16.77	17.28	15.43	18.38	18.39	19.78	16.01
CFPP	51.13	36.21	37.81	32	41.27	41.3	45.67	33.82
CP	13.98	8.32	8.06	6.56	6.04	6.40	8.08	6.43
APE	57.63	75.12	82.02	79.61	77.15	71.95	64.24	73.37
BAPE	28.83	29.01	33.07	29.88	29.56	26.38	23.51	26.11
OS (hours)	9.94	8.15	7.42	6.68	6.83	7.29	7.98	7.36
HHV (Mj Kg^{-1})	38.74	38.5	38.73	37.58	37.02	36.87	37.23	36.64
ν (mm^2 s^{-1})	1.37	1.35	1.36	1.31	1.3	1.3	1.32	1.28
ρ (g cm^{-3})	0.85	0.85	0.85	0.83	0.81	0.81	0.82	0.80

Notes: DU = degree of unsaturation, SV = saponification value, IV = iodine value, CN = cetane number, LCSF = long-chain saturated factor, CFPP = cold filter plugging point, CP = cloud point, APE = allylic position equivalents, BAPE = bis-allylic position equivalents, OS = oxidation stability, HHV = higher heating value, ν = kinematic viscosity, ρ = density. CP and CFPP are expressed in °C.

An additional practical aspect related to saline cultivation is the potential carryover of inorganic chloride salts into the harvested biomass or downstream lipid/FAME fractions. In the present study, biodiesel-related properties were predicted from the organic FAME composition. Therefore, the estimates do not account for possible residual chloride contamination. NaCl addition to the culture medium is not expected to chemically incorporate chlorine into FAME molecules, but incomplete removal of salts during harvesting, extraction, or purification could affect fuel quality and increase corrosion risk during processing, storage, or engine use. Consequently, the biodiesel-quality interpretation reported here should be considered compositional and predictive. Future work aimed at fuel production from saline-grown biomass should include biomass washing or desalting steps, chloride analysis of the lipid/FAME fraction, and verification of inorganic contaminants before assessing practical fuel compliance.

The analysis indicated that most derived fuel parameters complied with ASTM D6751-12 specifications [53], and several requirements of the European EN 14214 and EN 590 standards were also satisfied [54] (Table 4). Among the critical parameters, the cetane number (CN) is a key determinant of ignition quality. Biodiesel from *A. protothecoides* consistently exceeded the ASTM minimum threshold of 40, ranging from 56.07 (10 g L^{-1} NaCl) to 61.10 (45 g L^{-1} NaCl), reflecting favorable ignition behavior. Higher levels of saturated FAMEs typically increase CN, while unsaturation and chain branching reduce it. For instance, C18:0 is reported to have a CN of 86.9, whereas C18:1 has a lower CN of 59.3 [55]. In *A. protothecoides*, the balance of SFA and MUFA resulted in CN values comparable to or better than those of conventional feedstocks.

Viscosity (ν) and density (ρ) are also central to biodiesel quality. According to EN 14214, viscosity should fall between 3.5 and 5 mm^2 s^{-1} and density between 0.86 and 0.90 g cm^{-3}.

In this study, all treatments exhibited compliant density values, while viscosity values were consistently lower (1.28–1.37 mm^2 s^{-1}), including the control, suggesting the need for blending or additive use to reach the prescribed range. Importantly, viscosity correlates with both chain length and saturation: long-chain saturated FAMEs increase viscosity, while unsaturation reduces it. The relatively high UFA content in *A. protothecoides* lipids explains the lower viscosity observed, but this may also confer improved atomization and cold-start properties.

Oxidative stability (OS) is a critical parameter that is strongly influenced by the degree of unsaturation. While PUFAs such as C18:2 ω-6 and C18:3 ω-3 improve cold-flow properties, they reduce OS due to the presence of bisallylic carbons that are susceptible to oxidation. Consequently, the EN 14214 standard sets maximum limits for PUFA content. In *A. protothecoides*, PUFA levels reached up to 28.84% at 20 g L^{-1} NaCl, which could compromise long-term storage stability despite the generally favorable fuel profile. Notably, under 5 g L^{-1} NaCl, biodiesel exhibited an OS of 8.15 hours, meeting the European minimum requirement, along with a high CN (57.42), low iodine value (IV) (73.56 g I_2 100 g^{-1}), and improved cold-flow properties relative to the control.

Cold flow properties, represented by the cloud point (CP) and CFPP, are critical for ensuring biodiesel operability at low temperatures. Long-chain saturated FAMEs generally impair cold flow, whereas UFAs enhance it [9]. In the present study, the predicted CFPP values varied markedly among treatments and should not be described as uniformly low across the salinity gradient. The control showed the highest predicted CFPP value, 51.13 °C, indicating poor cold-flow performance. By contrast, salt-treated cultures showed lower predicted CFPP values, with the lowest value observed at 20 g L^{-1} NaCl, 32 °C. This reduction coincided with the salinity-induced decrease in SFAs, particularly C16:0, and the increase in unsaturated C18 FAs, especially C18:2 ω-6. Nevertheless, even the lowest predicted CFPP value remained positive, indicating that the produced FAME mixtures would still have limited cold-flow suitability without further improvement, such as blending with biodiesel fractions richer in unsaturated short-chain FAMEs or the use of cold-flow improvers. Therefore, the CFPP results should be interpreted as showing a relative improvement under moderate salinity, rather than full cold-flow compliance.

Other factors, such as lubricity and HHV, also influence biodiesel quality. Biodiesel typically exhibits excellent lubricating properties, often superior to those of fossil diesel due to its polar FAME components. HHV, however, is generally lower than that of fossil diesel because of its oxygenated nature, although it can vary depending on chain length and degree of unsaturation. The flash point, which is essential for safe storage and handling, remained within acceptable limits for all treatments, indicating effective removal of residual methanol. Since the ratio of SFAs and UFAs in the lipid profile strongly determines biodiesel quality and because salinity altered the relative FA composition, we calculated

biodiesel properties to assess the impact of salinity on IV, CFPP, and CN, all of which are closely associated with fuel performance. CN reflects ignition quality, with higher CN values corresponding to shorter ignition delays. IV indicates susceptibility to oxidative degradation and is influenced by the number and position of double bonds in the alkyl chains. CFPP represents low-temperature flow behavior and correlates with the proportion of UFAs in biodiesel [9,54].

It is important to distinguish between the salinity that optimizes growth performance and the salinity that provides the most favorable predicted biodiesel-quality profile. In the present study, these two optima did not coincide. The modeled optimum for specific growth rate occurred around 20 g L^{-1} NaCl, whereas the 5 g L^{-1} NaCl treatment provided the most favorable relative compromise among fuel-related properties, including cetane number, iodine value, oxidative stability, and cold-flow-related parameters. This difference reflects the fact that biomass accumulation and FAME quality are governed by different physiological and compositional responses to salinity. Therefore, the term "optimal" should be interpreted according to the target application. For biomass-oriented production, salinities around 10–20 g L^{-1} may be preferable, whereas for biodiesel-quality-oriented production, mild salinity around 5 g L^{-1} may be more advantageous. At industrial scale, however, salinity selection should be based on multi-objective optimization, integrating biomass productivity, lipid productivity, FAME composition, fuel-standard compliance, medium cost, water availability, and downstream processing requirements. Since none of the tested conditions fully satisfied all biodiesel-quality criteria, particularly viscosity, further optimization or blending would be required for direct fuel application.

In summary, *A. protothecoides* demonstrates strong potential as a biodiesel feedstock, producing fuel that largely complies with ASTM D6751 and partially with EN 14214 requirements. The best compromise between yield and fuel quality was achieved at 5 g L^{-1} NaCl, which provided optimal CN, OS, and cold-flow properties. While viscosity and long-term oxidative stability remain critical challenges, these can be mitigated through blending strategies or the addition of stabilizers. The modulation of FA composition by salinity highlights an opportunity to optimize culture conditions for targeted biodiesel properties, confirming the biotechnological relevance of this microalga.

3.3.2. Potential Applications in Non-Energetic Sectors

The salinity-induced modifications of the FAME profile substantially affected the potential oleochemical applications of *A. protothecoides* lipids. In particular, the intermediate salinity range (10–35 g L^{-1}) generated the most chemically reactive FAME mixtures, as demonstrated by the highest values of degree of unsaturation (DU = 81.0–82.9), iodine value (IV = 73.2–79.2 g I_2 100 g^{-1}), allylic position equivalents (APE = 77.1–82.0), and bis-allylic position equivalents (BAPE = 29.6–33.1) (Table 5). These parameters are directly associated with the density of carbon-carbon double bonds and allylic reactive sites available for chemical functionalization reactions. Consistently, the FA composition reported in Table S2 revealed a marked enrichment in linoleic acid, whose concentration increased from 12.99% in the control culture to a maximum of 28.84% at 20 g L^{-1}. Since PUFAs provide multiple reactive sites for epoxidation and subsequent ring-opening reactions, these salinity conditions appear particularly suitable for the production of epoxidized esters, bio-based plasticizers, polyols, and polyurethane intermediates [56,57]. Similar relationships between unsaturation degree and suitability for polymer-oriented oleochemistry have been extensively reported for vegetable- and microalgae-derived FAMEs, where highly unsaturated feedstocks are generally preferred for epoxidation, acrylation, and other double-bond functionalization routes [58,59].

The same compositional characteristics also suggest potential applications in coating and resin chemistry. The elevated IVs observed at 10–20 g L^{-1} indicate a greater abundance of reactive unsaturation compared with the control culture (60.96 g I_2 100 g^{-1}). Nevertheless, all IVs remained below 80 g I_2 100 g^{-1}, well below the typical range of classical drying oils such as linseed [60]. Therefore, although salinity increased the reactivity of the FAME mixtures, these lipids should be regarded as feedstocks for chemically modified coatings and alkyd resins rather than direct substitutes for conventional drying oils [61,62]. In this respect, the salinity range between 20 and 35 g L^{-1} appears to represent the most promising compromise between high double-bond density and preservation of the predominantly C16–C18 character of the lipid fraction.

A different application scenario emerged under high salinity stress (45–50 g L^{-1}), where the lipid profile shifted toward a more monounsaturated composition. The highest MUFA content (35.03%) and oleic acid concentration (23.87%) were observed at 50 g L^{-1}, while the UFA/SFA ratio reached 1.50, more than twice the value measured in the control culture (0.70). This shift toward oleic-rich FAME mixtures is particularly relevant for lubricant-oriented applications [63]. MUFAs are generally considered more attractive than polyunsaturated species for biolubricant production because they provide a favorable balance between oxidative stability and low-temperature fluidity [64]. In contrast, excessive PUFA contents tend to increase susceptibility to autoxidation [65], whereas highly saturated feedstocks often exhibit poor flow properties at low temperatures [9]. Consequently, the FAME mixtures obtained at 45–50 g L^{-1} appear especially suitable as precursors for the synthesis of biolubricants and lubricant base stocks after conventional upgrading steps such as transesterification with polyols, estolide formation, or other viscosity-enhancing modifications [64].

The enrichment in oleic acid observed at high salinity may also increase the attractiveness of these lipids for the production of specialty platform chemicals. Oleic acid is the traditional precursor for the synthesis of azelaic and pelargonic acids through oxidative cleavage processes, and oleic-rich feedstocks are generally preferred because they offer greater product selectivity than mixtures dominated by PUFAs [66]. In this respect, the 50 g L^{-1} condition appears particularly promising, combining the highest oleic acid concentration of the entire series with a still substantial fraction of unsaturated C18 chains. Conversely, although the 20–35 g L^{-1} treatments exhibited higher overall unsaturation, the larger contribution of linoleic acid would likely broaden the distribution of oxidation products and reduce selectivity toward the desired C9-C9 cleavage products.

The observed salinity-dependent changes are also relevant for more conventional oleochemical sectors, including soaps, fatty alcohols, fatty amides, and surfactant intermediates. Despite the strong remodeling of the saturation degree, the proportion of C16–C18 FAs remained remarkably constant across the entire salinity range, varying only between approximately 89 and 92% (Table 4). This indicates that salinity primarily affected desaturation pathways rather than chain-length distribution. Such a compositional stability is advantageous because C16–C18 FAs represent the dominant industrial feedstocks for a wide range of oleochemical products, including fatty alcohols, esterquats, metallic soaps, and methyl ester sulfonates [67]. From this perspective, the control culture and, to a lesser extent, the 45 g L^{-1} treatment may be considered the most attractive conditions for the production of conventional saturated-chain oleochemicals. These cultures exhibited the highest SFA contents (60.0 and 48.4%, respectively), together with the highest oxidation stability values (9.94 and 7.98 h) and the highest cetane numbers (59.85–61.10), all characteristics generally associated with greater storage stability and oxidative resistance.

Overall, the results demonstrate that salinity can be exploited as an effective tool for tailoring the oleochemical profile of *A. protothecoides* lipids toward specific industrial

applications. Intermediate salinities (10–35 g L^{-1}) favor the production of highly reactive PUFA-rich feedstocks suitable for epoxidized products, plasticizers, polyols, and polymer intermediates, whereas high salinities (45–50 g L^{-1}) promote the formation of oleic-rich FAME mixtures more appropriate for biolubricants and oleic-derived platform chemicals. In contrast, low-salinity conditions preserve a more saturated profile that is advantageous for the manufacture of conventional C16–C18 oleochemicals. These findings therefore support the concept of salinity-driven lipid engineering as a practical strategy for directing microalgal biorefineries toward distinct high-value oleochemical markets rather than exclusively targeting biodiesel production.

On the other hand, the practical advantage of salinity stress lies in its potential use as a controllable cultivation lever. Unlike nutrient starvation, which often strongly limits biomass production, moderate salinity may allow continued growth while inducing changes in lipid quality. In the present study, this was reflected by the different salinity optima observed for growth and predicted biodiesel quality. However, salinity should not be considered universally beneficial. Its industrial usefulness depends on identifying a compromise between biomass productivity, lipid productivity, FAME composition, medium cost, water source, and downstream processing requirements. Therefore, salinity stress should be viewed as a tuning strategy rather than as a simple method to maximize all production parameters simultaneously.

3.4. Comparative Relevance with Previous Literature

To clarify the specific contribution of the present work within the existing literature, Table 5 compares this study with representative previous research on microalgal lipid production, salinity stress, *A. protothecoides*, biodiesel-property prediction, oleochemical applications, and process-level considerations. The comparison highlights that most previous studies have focused on one or a few of these aspects separately, whereas the present study integrates growth modeling, lipid accumulation, FAME profile modulation, predicted biodiesel quality, and broader biorefinery implications under a controlled NaCl salinity gradient.

Overall, Table 5 shows that the usefulness of the present study lies in its integrated approach. While previous literature has demonstrated the relevance of microalgae for lipid production, wastewater cultivation, salinity stress responses, biodiesel-quality prediction, or oleochemical conversion, fewer studies have connected these aspects in a single experimental framework for *A. protothecoides*. The present work therefore contributes by identifying salinity as a possible cultivation lever to modulate both biomass-related parameters and lipid quality, while also recognizing that practical application requires further validation using real saline water matrices, scale-up trials, and dedicated techno-economic and life-cycle assessments.

Table 5. Comparison between the previous literature and the present study, highlighting the specific usefulness of the current research.

Literature Area	References	Main Contribution of Previous Literature	Main Limitation Relative to the Present Study	Specific Usefulness of the Present Study
General potential of microalgae for sustainable bioprocesses	[3,4]	Demonstrated the general relevance of microalgae for sustainability, biomass production, and process development.	These studies mainly provide broad conceptual or modeling frameworks and do not focus on salinity-driven FAME modulation in *A. protothecoides*.	The present study provides experimental evidence linking salinity, growth kinetics, lipid production, FAME composition, and predicted product quality in one strain-specific framework.

Table 5. *Cont.*

Literature Area	References	Main Contribution of Previous Literature	Main Limitation Relative to the Present Study	Specific Usefulness of the Present Study
Microalgae cultivation in wastewater or alternative water streams	[5–7,20]	Showed that microalgae can grow in low-quality waters or wastewater streams, supporting resource-efficient cultivation.	These studies mainly focus on nutrient removal, biomass production, or specific products, rather than on NaCl-driven salinity effects on FAME quality.	The present study evaluates whether salinity tolerance could support future cultivation in brackish, marine, or saline wastewater-based systems, while clarifying that this requires further validation using real water matrices.
Microalgal lipid production and cultivation-factor optimization	[2,8,10,41]	Demonstrated that cultivation conditions can influence growth, lipid synthesis, FAME profile, and biodiesel-related properties in different microalgae.	These works do not specifically test a broad NaCl salinity gradient in *A. protothecoides*.	The present study extends cultivation-factor optimization to salinity stress and combines lipid/FAME data with growth modeling and predicted biodiesel-quality assessment.
Salinity stress in microalgae other than *A. protothecoides*	[13–16,29,43,45,46,48]	Reported that salinity can affect growth, lipid accumulation, oxidative stress responses, and fatty-acid remodeling in several microalgal species.	The response to salinity is species-specific; therefore, results from *Chlorella*, *Scenedesmus*, *Dunaliella*, *Tetraselmis*, or *Chlamydomonas* cannot be directly transferred to *A. protothecoides*.	The present study provides species-specific data for *A. protothecoides* across 0–50 g L^{-1} NaCl, identifying different salinity optima for growth and predicted biodiesel quality.
Strain-specific studies on *A. protothecoides*	[18–21]	Demonstrated the oleaginous character, metabolic flexibility, wastewater compatibility, industrial fermentation potential, and molecular basis of oil accumulation in *A. protothecoides* or its former *Chlorella protothecoides* classification.	Most studies focus on heterotrophic or mixotrophic cultivation, glycerol/wastewater use, industrial fermentation, or omics analysis; salinity-driven growth/FAME modulation remains less explored.	The present study specifically investigates salinity as a controlled abiotic factor affecting growth kinetics, lipid accumulation, FAME profile, and predicted fuel properties in *A. protothecoides*.
Biodiesel-property estimation from FAME composition	[1,9,28,52,54,55,60]	Established the importance of FAME composition for cetane number, viscosity, iodine value, oxidative stability, cold-flow behavior, and biodiesel-standard compliance.	These studies mainly provide general biodiesel-quality frameworks or prediction tools and are not directly linked to salinity-controlled cultivation of *A. protothecoides*.	The present study connects salinity-induced FAME shifts with predicted biodiesel properties and explicitly identifies partial rather than full compliance with EN 14214/ASTM D6751.
Oleochemical applications of lipid/FAME fractions	[11,12,56,58,59,61,63,64,67,68]	Highlighted the potential of biological lipids and FAMEs as feedstocks for lubricants, surfactants, coatings, polymers, epoxy resins, and other bio-based chemicals.	These studies generally focus on downstream oleochemical conversion or product applications, rather than on cultivation strategies to tune the upstream FAME profile.	The present study suggests that salinity can be used as an upstream cultivation lever to modify the C16–C18 saturated/unsaturated FAME balance, potentially supporting biodiesel and non-fuel oleochemical applications.
Techno-economic and environmental considerations	[17,68–70]	Emphasized that microalgal biofuel and biorefinery systems require evaluation of process costs, water use, harvesting, downstream processing, LCA, and scale-up feasibility.	These studies provide process-level assessment but do not experimentally test salinity-driven lipid modulation in *A. protothecoides*.	The present study provides experimental data useful for future process assessment, while recognizing that water-footprint reduction, LCA, and techno-economic feasibility were not quantified and require dedicated future studies.

3.5. Practical Implications, Techno-Economic Considerations, and Future Research Directions

The present study shows that salinity can be used as a cultivation variable to modulate both growth dynamics and FAME composition in *A. protothecoides*. However, the transfer of this strategy from laboratory-scale cultivation to industrial production requires careful consideration of several technical and economic factors [69]. First, the use of NaCl-supplemented medium in controlled laboratory experiments should be considered a simplified model of salinity stress rather than a direct representation of real brackish water, seawater, or saline wastewater. At industrial scale, the composition of saline water sources may vary considerably and may include additional ions, organic matter, suspended solids, or potential contaminants that can affect algal growth, lipid accumulation, harvesting efficiency, and downstream processing [6,7,10]. Therefore, the results obtained using NaCl alone should be validated using real saline water matrices.

Second, the economic benefit of salinity-based cultivation depends on whether saline water sources can reduce freshwater demand and medium-preparation costs without introducing additional expenses [70]. Potential advantages include the partial replacement of freshwater, improved compatibility with brackish or marine water resources, and possible integration with saline waste streams. However, these benefits may be offset by costs associated with water pretreatment, sterilization or contamination control, corrosion-resistant materials, salt accumulation during water recycling, and management of saline effluents [69]. In addition, higher salinity may affect pumping, mixing, harvesting, biomass washing, and solvent-extraction steps, all of which must be considered in process-scale design [1]. It should also be considered that when saline cultivation is linked to biodiesel production, residual chloride salts must be removed or monitored because chloride carry-over can contribute to corrosion and fuel-quality problems during downstream processing, storage, and use.

A further techno-economic limitation concerns the final application of the lipid fraction. Although mild salinity improved some predicted biodiesel-related properties, none of the tested conditions fully satisfied all fuel-standard requirements, particularly because the estimated viscosity values remained below the EN 14214 range. Therefore, direct biodiesel production from the obtained FAME mixtures may require blending with other lipid feedstocks, antioxidant addition, cold-flow or viscosity adjustment, or downstream upgrading [1]. Alternatively, the salinity-modulated FAME profiles may be more suitable for broader oleochemical applications, where specific C16–C18 SFA and UFA fractions can be exploited for the production of biodegradable lubricants, surfactants, plasticizers, coatings, or polymer precursors [68].

Future research should therefore focus on multi-objective optimization rather than on a single performance parameter [2,10,69]. In particular, salinity should be optimized by jointly considering biomass productivity, lipid productivity, FAME composition, water source, medium cost, harvesting efficiency, downstream processing, and final product specifications. Further work should also include long-term cultivation trials, semi-continuous or continuous operation, validation in larger photobioreactors, testing with real brackish water, seawater, or saline wastewater, and assessment of salt accumulation during medium recycling. Finally, dedicated life-cycle assessment and techno-economic analysis will be required to determine whether salinity-based cultivation of *A. protothecoides* can provide measurable environmental and economic advantages at industrial scale [1].

Table 6 summarizes a brief analysis of the industrial potential of FAMEs obtained from *A. protothecoides* cultivated under different salinity levels.

Table 6. Recommended NaCl concentration for specific industrial sectors: advantages, limitations and applicability.

Target Application	[NaCl] (g L^{-1})	Experimental Basis	Advantages	Limitations	Applicability
Biodiesel	5	High biomass productivity; balanced FAME profile; favorable CN, IV and OS	Best productivity–fuel quality compromise	Low predicted viscosity and poor cold-flow properties require blending or upgrading	Best condition tested for biodiesel production
Maximum lipid/FAME feedstock production	10	Highest biomass and lipid productivity	Maximizes feedstock yield	Less balanced fuel properties than 5 g L^{-1}	Preferred when production yield is prioritized
Epoxidized FAMEs, plasticizers, polyols and polyurethane intermediates	10–20	High unsaturation and reactive-site density	Favors epoxidation and functionalization	Lower oxidative stability; stabilization may be required	Promising for polymer-oriented applications
Modified coatings and resin precursors	10–20	High IV and PUFA content	Good potential for chemical crosslinking	Requires chemical modification; unsuitable as a direct drying oil	Suitable as a functionalized resin precursor
Biolubricants and lubricant base stocks	45–50	Highest MUFA and oleic acid contents	Good balance of fluidity and oxidative stability after conversion	Low biomass productivity and high salt-management costs	Suitable mainly for high-value or two-stage production
Oleic-derived platform chemicals	50	Highest oleic acid content	Favors production of azelaic and pelargonic acids	Requires selective conversion or fractionation	Potential specialty-chemical application
Soaps, fatty alcohols, amides and surfactant intermediates	0–5	High C16–C18 and SFA contents	Good storage and oxidative stability	Must compete with established vegetable-oil feedstocks	5 g L^{-1} offers the best practical compromise
Hydroprocessed aviation-fuel intermediates	5–10	High productivity and predominantly C16–C18 FAMEs	Suitable lipid feedstock for HEFA-type processing	Requires hydrogenation, deoxygenation and chain-length adjustment	Technically feasible but not demonstrated here

4. Conclusions

This study demonstrates that salinity is a critical factor shaping both the growth performance and lipid composition of *Auxenochlorella protothecoides*, with direct consequences for its suitability as a biodiesel feedstock. The strain exhibited a halotolerant behavior, achieving its best performance at moderate salt concentrations (10–20 g L^{-1} NaCl), where biomass accumulation and productivity were maximized. At the same time, salinity stress induced marked shifts in the FA profile, reducing the relative abundance of saturated species such as C16:0 while favoring the accumulation of UFAs, particularly oleic (C18:1 ω-9) and linoleic (C18:2 ω-6) acids. These changes, while beneficial for properties like cetane number and cold-flow performance, also introduced limitations in oxidative stability due to the elevated polyunsaturated content. The integration of growth and lipid data into biodiesel property predictions suggests that mild salinity levels, especially around 5 g L^{-1} NaCl, offer the most favorable compromise between productivity and fuel quality, yielding biodiesel that aligns more closely with international standards. Nonetheless, viscosity values remained consistently below European requirements, and long-term stability concerns persist. These findings underline the dual role of salinity as both an enhancer of biomass performance and a modulator of lipid quality, reinforcing its potential as a cultivation lever for tailoring biofuel characteristics. Overall, *A. protothecoides* confirms its promise as a microalgal platform for sustainable biodiesel production, but the results also highlight the necessity of complementary strategies such as mixotrophic growth, wastewater utilization, or strain selection to overcome current limitations. By strategically combining cultivation approaches, it may be possible to achieve both regulatory compliance and industrial competitiveness, ultimately strengthening the role of microalgae in the renewable energy

landscape. Beyond biodiesel production, the observed salinity-dependent modulation of the FAME profile also suggests potential opportunities in the oleochemical sector, particularly for the production of biodegradable lubricants, surfactants and bio-based polymer precursors. These findings reinforce the possibility of integrating *A. protothecoides* cultivation within a broader microalgal biorefinery concept, where salinity could be exploited as a low-cost operational parameter to tailor lipid composition toward specific industrial targets. Furthermore, the ability of *A. protothecoides* to maintain substantial growth under saline conditions supports the possibility of exploiting seawater or low-quality saline streams for cultivation, thereby potentially decreasing freshwater consumption and improving the environmental sustainability of the process. In this sense, salinity may represent not only a metabolic stressor capable of tailoring lipid composition, but also an operational lever contributing to the reduction in the overall water footprint of industrial microalgal production.

Supplementary Materials: The following supporting information can be downloaded at https://www.mdpi.com/article/10.3390/app16157857/s1.

Author Contributions: Conceptualization and design, T.M., F.S., G.A.L., A.C.; data curation, T.M., G.A.L.; formal analysis, T.M., S.M., V.L., F.S.; writing—original draft preparation, G.A.L., S.M., A.P., A.C.; writing—review and editing, G.A.L., A.C.; supervision, A.C., F.S. All authors have read and agreed to the published version of the manuscript.

Funding: This research received no external funding.

Institutional Review Board Statement: Not applicable.

Informed Consent Statement: Not applicable.

Data Availability Statement: The raw data supporting the conclusions of this article will be made available by the authors on request.

Acknowledgments: During the preparation of this work, the authors used ChatGPT 5.5 in order to rephrase some written paragraphs, with the sole aim of making the whole manuscript more fluent and readable. After using this tool/service, the authors reviewed and edited the content as needed and take full responsibility for the content of the published article.

Conflicts of Interest: Author Samaneh Mohammadnejad and Giovanni Antonio Lutzu were employed by the company Teregroup Srl. The remaining authors declare that the research was conducted in the absence of any commercial or financial relationships that could be construed as a potential conflict of interest.

References

1. Wan Osman, W.N.A.; Rosli, M.H.; Mazli, W.N.A.; Samsuri, S. Comparative review of biodiesel production and purification. *Carbon Capture Sci. Technol.* **2024**, *13*, 100264. [CrossRef]
2. Concas, A.; Malavasi, V.; Costelli, C.; Fadda, P.; Pisu, M.; Cao, G. Autotrophic growth and lipid production of *Chlorella sorokiniana* in lab batch and BIOCOIL photobioreactors: Experiments and modeling. *Bioresour. Technol.* **2016**, *211*, 327–338. [CrossRef] [PubMed]
3. Usai, A.; Theodoropoulos, C.; Di Caprio, F.; Altimari, P.; Cao, G.; Concas, A. Structured population balances to support microalgae-based processes: Review of the state-of-art and perspectives analysis. *Comput. Struct. Biotechnol. J.* **2023**, *21*, 1169–1188. [CrossRef] [PubMed]
4. Hosny, S.; Elshobary, M.E.; El-Sheekh, M.M. Unleashing the power of microalgae: A pioneering path to sustainability and achieving the sustainable development goals. *Environ. Sci. Pollut. Res.* **2025**, *32*, 17312–17342. [CrossRef] [PubMed]
5. Concas, A.; Lutzu, G.A.; Turgut Dunford, N. Experiments and modeling of *Komvophoron* sp. growth in hydraulic fracturing wastewater. *Chem. Eng. J.* **2021**, *426*, 131299. [CrossRef]
6. Lutzu, G.A.; Marin, M.A.; Concas, A.; Dunford, N.T. Growing *Picochlorum oklahomensis* in hydraulic fracturing wastewater supplemented with animal wastewater. *Water Air Soil Pollut.* **2020**, *231*, 457. [CrossRef]

7. Lutzu, G.A.; Concas, A.; Damergi, E.; Chen, L.; Zhang, W.; Liu, T. Production of carotenoids and astaxanthin from *Haematococcus pluvialis* cultivated under mixotrophy using brewery wastewater: Effect of light intensity and cultivation time. *Appl. Sci.* **2024**, *14*, 9704. [CrossRef]
8. Vitali, L.; Lolli, V.; Sansone, F.; Concas, A.; Lutzu, G.A. Effect of mixotrophy on lipid content and fatty acids methyl esters profile by *Chromochloris zofingiensis* grown in media containing sugarcane molasses. *BioEnergy Res.* **2023**, *16*, 1851–1861. [CrossRef]
9. Pradana, Y.S.; Makertihartha, I.G.B.N.; Indarto, A.; Prakoso, T.; Soerawidjaja, T.H. A review of biodiesel cold flow properties and its improvement methods: Towards sustainable biodiesel application. *Energies* **2024**, *17*, 4543. [CrossRef]
10. Concas, A.; Steriti, A.; Pisu, M.; Cao, G. Experimental and theoretical investigation of the effects of iron on growth and lipid synthesis of microalgae in view of their use to produce biofuels. *J. Environ. Chem. Eng.* **2021**, *9*, 105349. [CrossRef]
11. Lomanar, M.L.; Timmers, R.A.; Levío-Raimán, M.; González-Fernández, C.; Moreno, A.D.; Negro, M.J. Oleochemicals production from microalgae and yeast. In *Eukaryotic Microorganisms as Sources of Bioproducts*; Woodhead Publishing: Cambridge, UK, 2025.
12. Campanella, A.; Rustoy, E.; Baldessari, A.; Baltanás, M.A. Lubricants from chemically modified vegetable oils. *Bioresour. Technol.* **2010**, *101*, 245–254. [CrossRef] [PubMed]
13. Pandit, P.R.; Fulekar, M.H.; Karuna, M.S.L. Effect of salinity stress on growth, lipid productivity, fatty acid composition, and biodiesel properties in *Acutodesmus obliquus* and *Chlorella vulgaris*. *Environ. Sci. Pollut. Res.* **2017**, *24*, 13437–13451. [CrossRef] [PubMed]
14. Macías-de la Rosa, A.; López-Rosales, L.; Contreras-Gómez, A.; Sánchez-Mirón, A.; García-Camacho, F.; Cerón-García, M.C. Salinity as an abiotic stressor for eliciting bioactive compounds in marine microalgae. *Toxins* **2024**, *16*, 425. [CrossRef] [PubMed]
15. Singh, R.P.; Yadav, P.; Kumar, A.; Hashem, A.; Avila-Quezada, G.D.; Abd_Allah, E.F.; Gupta, R.K. Salinity-induced physiochemical alterations to enhance lipid content in oleaginous microalgae *Scenedesmus* sp. BHU1 via two-stage cultivation for biodiesel feedstock. *Microorganisms* **2023**, *11*, 2064. [CrossRef] [PubMed]
16. Fal, S.; Aasfar, A.; Rabie, R.; Smouni, A.; El Arroussi, H. Salt-induced oxidative stress alters physiological, biochemical and metabolomic responses of the green microalga *Chlamydomonas reinhardtii*. *Heliyon* **2022**, *8*, e08811. [CrossRef] [PubMed]
17. Moradiya, K.K.; Marathe, K.V. Life Cycle Assessment (LCA) of marine microalgae cultivation and harvesting process for the Indian context. *Sustain. Energy Technol. Assess.* **2023**, *56*, 103063. [CrossRef]
18. Korozi, E.; Tsagou, V.; Kefalogianni, I.; Markou, G.; Antonopoulos, D.; Chakalis, L.; Kotzamanis, Y.; Chatzipavlidis, I. Continuous culture of *Auxenochlorella protothecoides* on biodiesel derived glycerol under mixotrophic and heterotrophic conditions: Growth parameters and biochemical composition. *Microorganisms* **2022**, *10*, 541. [CrossRef] [PubMed]
19. Xiao, Y.; Lu, Y.; Dai, J.; Wu, Q. Industrial fermentation of *Auxenochlorella protothecoides* for production of biodiesel and its application in vehicle diesel engines. *Front. Bioeng. Biotechnol.* **2015**, *3*, 164. [CrossRef] [PubMed]
20. Zhou, W.; Li, Y.; Min, M.; Hu, B.; Zhang, H.; Ma, X.; Li, L.; Cheng, Y.; Chen, P.; Ruan, R. Growing wastewater-born microalga *Auxenochlorella protothecoides* UMN280 on concentrated municipal wastewater for simultaneous nutrient removal and energy feedstock production. *Appl. Energy* **2012**, *98*, 433–440. [CrossRef]
21. Gao, C.; Wang, Y.; Shen, Y.; Yan, D.; He, X.; Dai, J.; Wu, Q. Oil accumulation mechanisms of the oleaginous microalga *Chlorella protothecoides* revealed through its genome, transcriptomes, and proteomes. *BMC Genom.* **2014**, *15*, 582. [CrossRef] [PubMed]
22. Costa, G.d.S.; Martinez-Burgos, W.J.; dos Reis, G.A.; Puche, Y.P.; Vega, F.R.; Rodrigues, C.; Serra, J.L.; Campos, S.d.M.; Soccol, C.R. Advances in biomass and microbial lipids production: Trends and prospects. *Processes* **2024**, *12*, 2903. [CrossRef]
23. Bligh, E.G.; Dyer, W.J. A rapid method of total lipid extraction and purification. *Can. J. Biochem. Physiol.* **1959**, *37*, 911–917. [CrossRef]
24. Chen, L.; Liu, T.; Zhang, W.; Chen, X.; Wang, J. Biodiesel production from algae oil high in free fatty acids by two-step catalytic conversion. *Bioresour. Technol.* **2012**, *111*, 208–214. [CrossRef] [PubMed]
25. Lage, S.; Gentili, F.G. Quantification and characterisation of fatty acid methyl esters in microalgae: Comparison of pretreatment and purification methods. *Bioresour. Technol.* **2018**, *257*, 121–128. [CrossRef] [PubMed]
26. Virtanen, P.; Gommers, R.; Oliphant, T.E.; Haberland, M.; Reddy, T.; Cournapeau, D.; Burovski, E.; Peterson, P.; Weckesser, W.; Bright, J.; et al. SciPy 1.0: Fundamental algorithms for scientific computing in Python. *Nat. Methods* **2020**, *17*, 261–272. [CrossRef] [PubMed]
27. Senthamilselvi, D.; Kalaiselvi, T. Fuel Properties of Fatty Acid Methyl Esters (FAME) Produced with Fats of Gamma—Irradiated Mutants of Oleaginous Microalga—*Chlorella* sp. KM504965. *Madras Agric. J.* **2022**, *109*, 28–35. [CrossRef]
28. Talebi, A.F.; Tabatabaei, M.; Chisti, Y. BiodieselAnalyzer: A user-friendly software for predicting the properties of prospective biodiesel. *Biofuel Res. J.* **2014**, *1*, 55–57. [CrossRef]
29. Sánchez-Alvarez, E.L.; González-Ledezma, G.; Bolaños Prats, J.A.; Stephano-Hornedo, J.L.; Hildebrand, M. Evaluating *Marinichlorella kaistiae* KAS603 cell size variation, growth and TAG accumulation resulting from rapid adaptation to highly diverse trophic and salinity cultivation regimes. *Algal Res.* **2017**, *25*, 12–24. [CrossRef]

30. Wang, T.; Ge, H.; Liu, T.; Tian, X.; Wang, Z.; Guo, M.; Chu, J.; Zhuang, Y. Salt stress induced lipid accumulation in heterotrophic culture cells of *Chlorella protothecoides*: Mechanisms based on the multi-level analysis of oxidative response, key enzyme activity and biochemical alteration. *J. Biotechnol.* **2016**, *228*, 18–27. [CrossRef] [PubMed]
31. Shetty, P.; Gitau, M.M.; Maróti, G. Salinity stress responses and adaptation mechanisms in eukaryotic green microalgae. *Cells* **2019**, *8*, 1657. [CrossRef] [PubMed]
32. Hu, Q. Environmental effects on cell composition. In *Handbook of Microalgal Culture: Applied Phycology and Biotechnology*, 2nd ed.; John Wiley & Sons, Ltd.: Hoboken, NJ, USA, 2013.
33. Roleda, M.Y.; Slocombe, S.P.; Leakey, R.J.; Day, J.G.; Bell, E.M.; Stanley, M.S. Effects of temperature and nutrient regimes on biomass and lipid production by six oleaginous microalgae in batch culture employing a two-phase cultivation strategy. *Bioresour. Technol.* **2013**, *129*, 439–449. [CrossRef] [PubMed]
34. Converti, A.; Casazza, A.A.; Ortiz, E.Y.; Perego, P.; Del Borghi, M. Effect of temperature and nitrogen concentration on the growth and lipid content of *Nannochloropsis oculata* and *Chlorella vulgaris* for biodiesel production. *Chem. Eng. Process. Process Intensif.* **2009**, *48*, 1146–1151. [CrossRef]
35. Kirst, G.O. Salinity tolerance of eukaryotic marine algae. *Annu. Rev. Plant Physiol. Plant Mol. Biol.* **1990**, *41*, 21–53. [CrossRef]
36. Hu, Q.; Sommerfeld, M.; Jarvis, E.; Ghirardi, M.; Posewitz, M.; Seibert, M.; Darzins, A. Microalgal triacylglycerols as feedstocks for biofuel production: Perspectives and advances. *Plant J.* **2008**, *54*, 621–639. [CrossRef] [PubMed]
37. Yadav, A.; Sharma, S.; Nitesh; Meena, R.; Bhardwaj, R.; Swapnil, P.; Meena, M. Tapping the microalgal potential: Genetic precision and stress-induction for enhanced astaxanthin and biofuel production. *Biotechnol. Biofuels Bioprod.* **2025**, *18*, 92. [CrossRef] [PubMed]
38. Mixson Byrd, S.; Burkholder, J.A.M.; Zimba, P.V. Environmental stressors and lipid production by *Dunaliella* Spp. I. Salinity. *J. Exp. Mar. Bio. Ecol.* **2017**, *487*, 18–32. [CrossRef]
39. El-Sheekh, M.M.; Galal, H.R.; Mousa, A.S.H.; Farghl, A.A.M. Impact of macronutrients and salinity stress on biomass and biochemical constituents in *Monoraphidium braunii* to enhance biodiesel production. *Sci. Rep.* **2024**, *14*, 2725. [CrossRef] [PubMed]
40. Morales, M.; Aflalo, C.; Bernard, O. Microalgal lipids: A review of lipids potential and quantification for 95 phytoplankton species. *Biomass Bioenergy* **2021**, *150*, 106108. [CrossRef]
41. Miotti, T.; Sansone, F.; Lolli, V.; Concas, A.; Lutzu, G.A. Mixotrophic and heterotrophic metabolism in brewery wastewater by *Chlorella vulgaris*: Effect on growth, FAME profile and biodiesel properties. *Chem. Eng. Trans.* **2024**, *109*, 97–102. [CrossRef]
42. The, K.Y.; Loh, S.H.; Aziz, A.; Takahashi, K.; Effendy, A.W.M.; Cha, T.S. Lipid accumulation patterns and role of different fatty acid types towards mitigating salinity fluctuations in *Chlorella vulgaris*. *Sci. Rep.* **2021**, *11*, 438. [CrossRef] [PubMed]
43. Los, D.A.; Murata, N. Membrane fluidity and its roles in the perception of environmental signals. *Biochim. Biophys. Acta-Biomembr.* **2004**, *1666*, 142–157. [CrossRef] [PubMed]
44. Ho, S.-H.; Ye, X.; Hasunuma, T.; Chang, J.-S.; Kondo, A. Perspectives on engineering strategies for improving biofuel production from microalgae. A critical review. *Biotechnol. Adv.* **2014**, *32*, 1448–1459. [CrossRef] [PubMed]
45. Salama, E.-S.; Kim, H.-C.; Abou-Shanab, R.A.I.; Ji, M.-K.; Oh, Y.-K.; Kim, S.-H.; Jeon, B.-H. Biomass, lipid content, and fatty acid composition of freshwater *Chlamydomonas mexicana* and *Scenedesmus obliquus* grown under salt stress. *Bioprocess Biosyst. Eng.* **2013**, *36*, 827–833. [CrossRef] [PubMed]
46. Saadaoui, I.; Cherif, M.; Siddiqui, S.A.; El Anbari, M.; Masmoudi, F.; Al Jabri, H. Abiotic stress applied to *Tetraselmis subcordiformis* reveals enhanced metabolic responses and increased production of omega-3 fatty acids: A metabolomic approach. *Algal Res.* **2024**, *77*, 103338. [CrossRef]
47. Wu, T.; Yu, L.; Zhang, Y.; Liu, J. Characterization of fatty acid desaturases reveals stress-induced synthesis of C18 unsaturated fatty acids enriched in triacylglycerol in the oleaginous alga *Chromochloris zofingiensis*. *Biotechnol. Biofuels* **2021**, *14*, 184. [CrossRef] [PubMed]
48. Chen, H.; Jiang, J.G. Osmotic responses of *Dunaliella* to the changes of salinity. *J. Cell. Physiol.* **2009**, *219*, 251–258. [CrossRef] [PubMed]
49. Sukenik, A. Ecophysiological considerations in the optimization of eicosapentaenoic acid production by *Nannochloropsis* sp. (Eustigmatophyceae). *Bioresour. Technol.* **1991**, *35*, 263–269. [CrossRef]
50. Hu, H.; Gao, K. Response of growth and fatty acid compositions of *Nannochloropsis* sp. to environmental factors under elevated CO_2 concentration. *Biotechnol. Lett.* **2006**, *28*, 987–992. [CrossRef] [PubMed]
51. Guschina, I.A.; Harwood, J.L. Lipids and lipid metabolism in eukaryotic algae. *Prog. Lipid Res.* **2006**, *45*, 160–186. [CrossRef] [PubMed]
52. Tamilselvan, P.; Sassykova, L.; Prabhahar, M.; Bhaskar, K.; Kannayiram, G.; Subramanian, S.; Prakash, S. Influence of saturated fatty acid material composition in biodiesel on its performance in internal combustion engines. *Mater. Today Proc.* **2020**, *33*, 1181–1186. [CrossRef]
53. Bi, C.H.; Min, M.; Nie, Y.; Xie, Q.L.; Lu, Q.; Deng, X.Y.; Anderson, E.; Li, D.; Chen, P.; Ruan, R. Process development for scum to biodiesel conversion. *Bioresour. Technol.* **2015**, *185*, 185–193. [CrossRef] [PubMed]

54. Barabas, I.; Todoru, I.-A. Biodiesel quality, standards and properties. In *Biodiesel-Quality, Emissions and By-Products*; IntechOpen: London, UK, 2011.
55. Knothe, G.; Razon, L.F. Biodiesel fuels. *Prog. Energy Combust. Sci.* **2017**, *58*, 36–59. [CrossRef]
56. Moser, B.R.; Cermak, S.C.; Doll, K.M.; Kenar, J.A.; Sharma, B.K. A review of fatty epoxide ring opening reactions: Chemistry, recent advances, and applications. *JAOCS J. Am. Oil Chem. Soc.* **2022**, *99*, 801–842. [CrossRef]
57. Re, R.N.; Hudecek, C.; Jaisingh, A.; Halloran, M.W.; Bruckbauer, A.; Wnuk-Fink, K.M.J.; Dev, A.; Harwich, N.; Subileau, M.; La Clair, J.J.; et al. Co-catalyst enabled biotransformation of polyunsaturated fatty acids for biobased monomers. *Org. Process Res. Dev.* **2025**, *29*(9), 2265–2274. [CrossRef]
58. Hess, S.K.; Lepetit, B.; Kroth, P.G.; Mecking, S. Production of chemicals from microalgae lipids—Status and perspectives. *Eur. J. Lipid Sci. Technol.* **2018**, *120*, 1700152. [CrossRef]
59. Hidalgo, P.; Álvarez, S.; Hunter, R.; Sánchez, A. Epoxidation of fatty acid methyl esters derived from algae biomass to develop sustainable bio-based epoxy resins. *Polymers* **2020**, *12*, 2313. [CrossRef]
60. Giakoumis, E.G. Analysis of 22 vegetable oils' physico-chemical properties and fatty acid composition on a statistical basis, and correlation with the degree of unsaturation. *Renew. Energy* **2018**, *126*, 403–419. [CrossRef]
61. Meier, M.A.R.; Metzger, J.O.; Schubert, U.S. Plant oil renewable resources as green alternatives in polymer science. *Chem. Soc. Rev.* **2007**, *36*, 1788–1802. [CrossRef]
62. Stenberg, C.; Svensson, M.; Johansson, M. A Study of the drying of linseed oils with different fatty acid patterns using RTIR-spectroscopy and chemiluminescence (CL). *Ind. Crops Prod.* **2005**, *21*, 263–272. [CrossRef]
63. Pawar, R.V.; Hulwan, D.B. Rheological, thermal and tribological performance of trimethylolpropane esters derived from high oleic non-edible oils: A sustainable biolubricant for industrial applications. *Biomass Convers. Biorefin.* **2025**, *15*, 25063–25092. [CrossRef]
64. Nguyen, D.T.; Silitonga, A.S.; Johir, M.A.H.; Cai, Z.; Kuzhiumparambil, U.; Ralph, P.; Nghiem, L.D. Species selection, scale-up cultivation, and oil characterization of microalgae for sustainable biolubricant production. *ACS Sustain. Chem. Eng.* **2026**, *14*, 7963–7973. [CrossRef]
65. Kaur, M.; Bhatia, S.; Bayram, I.; Decker, E.A.; Phutela, U.G. Oxidative stability of emulsions made with self-extracted oil from euryhaline microalgae *Spirulina* and *Scenedesmus*. *Algal Res.* **2023**, *75*, 103280. [CrossRef]
66. Ciriminna, R.; Fidalgo, A.; Ilharco, L.M.; Pagliaro, M. Herbicides based on pelargonic acid: Herbicides of the bioeconomy. *Biofuels Bioprod. Biorefin.* **2019**, *13*, 1476–1482. [CrossRef]
67. Biermann, U.; Bornscheuer, U.; Meier, M.A.R.; Metzger, J.O.; Schäfer, H.J. Oils and fats as renewable raw materials in chemistry. *Angew. Chem.-Int. Ed.* **2011**, *50*, 3854–3871. [CrossRef] [PubMed]
68. Beattie, A.; Vermaas, W.; Darzins, A.; Holland, S.C.; Li, S.; McGowen, J.; Nielsen, D.; Quinn, J.C. A probabilistic economic and environmental impact assessment of a cyanobacteria-based biorefinery. *Algal Res.* **2021**, *59*, 102454. [CrossRef]
69. Geng, Y.; Shaukat, A.; Azhar, W.; Raza, Q.U.; Tahir, A.; Abideen, M.Z.U.; Zia, M.A.B.; Bashir, M.A.; Rehim, A. Microalgal biorefineries: A systematic review of technological trade-offs and innovation pathways. *Biotechnol. Biofuels Bioprod.* **2025**, *18*, 93. [CrossRef] [PubMed]
70. Nogales-Delgado, S. Biodiesel production and Life Cycle Assessment: Status and prospects. *Energies* **2025**, *18*, 3338. [CrossRef]

Disclaimer/Publisher's Note: The statements, opinions and data contained in all publications are solely those of the individual author(s) and contributor(s) and not of MDPI and/or the editor(s). MDPI and/or the editor(s) disclaim responsibility for any injury to people or property resulting from any ideas, methods, instructions or products referred to in the content.